Phage CRISPR-like regulatory RNAs silence bacterial adaptive and innate immunity

Chao Liu[1,2†], Rui Wang[1†], Zhihua Li[1,2†], Wenhe Wang[3†], Jiachen Yao[4], Feiyue Cheng[1], Xiaoyu Du[5], Linlin Guan[5], Mario Rodríguez Mestre[4], Jing Xu[1,2], Qiong Xue[1], Jun Du[1,2], Tao Zhou[6], Xian Shu[1], Huiwei Zhao[1], Yue Feng[5*], Rafael Pinilla-Redondo[4*], Ming Li[1,2*]

[1]CAS Key Laboratory of Microbial Physiological and Metabolic Engineering, State Key Laboratory of Microbial Resources, Institute of Microbiology, Chinese Academy of Sciences, Beijing, China.
[2]College of Life Science, University of Chinese Academy of Sciences, Beijing, China.
[3]Ministry of Education Key Laboratory of Protein Science, Beijing Advanced Innovation Center for Structural Biology, Beijing Frontier Research Center for Biological Structure, School of Life Sciences, Tsinghua University, Tsinghua-Peking Center for Life Sciences, Beijing, China
[4]Section of Microbiology, Department of Biology, University of Copenhagen, Copenhagen, Denmark
[5]Beijing Advanced Innovation Center for Soft Matter Science and Engineering, Beijing Key Laboratory of Bioprocess, State Key Laboratory of Chemical Resource Engineering, College of Life Science and Technology, Beijing University of Chemical Technology, Beijing, China
[6]School of Life Sciences, Shandong Agricultural University, Taian, Shandong, China
[†]These authors contributed equally to this work.
*Corresponding authors. Email: lim_im@im.ac.cn (M. L.); rafael.pinilla@bio.ku.dk (R. P.-R.); fengyue@mail.buct.edu.cn (Y. F.).

Abstract: In prokaryotes, arrayed CRISPR RNAs (crRNAs) guide Cas proteins to destroy phage DNA/RNA, while solitary crRNA-like RNAs (crlRNAs) program Cas proteins for auto-regulation or to control abortive infection (Abi)-inducing toxins that activate when CRISPR-Cas fails. Here, we report that phages exploit crlRNA mimics to hijack these multi-layered host defenses. *Pseudomonas aeruginosa* phages use crlRNAs to thwart CRISPR-Cas immunity by inhibiting Cas expression, or to block Abi by silencing an unprecedented RNA toxin that features consecutive proline codons. Remarkably, the anti-CRISPR protein AcrIF24 selectively inhibits Cas proteins loaded with host crRNAs/crlRNAs, while allowing those complexed with viral crlRNAs to synergistically block Abi responses, as viral crlRNAs have co-adaptively evolved shorter spacer sequences. Furthermore, viral crlRNAs frequently organize as multiplexed arrays, mirroring the architecture of bacterial CRISPRs. Our findings showcase how phage RNAs hijack Cas proteins to silence multi-layered bacterial defenses, and highlight the delicate synergy between RNA and protein-based anti-CRISPR strategies.

Key words: CRISPR-Cas, abortive infection, anti-CRISPR, small RNA, RNA toxin

In prokaryotes, CRISPR-Cas systems provide adaptive immunity against invasive mobile genetic elements (MGEs), such as phages and plasmids. (*1-3*). These diverse systems are classified into two main groups (class 1 and class 2), encompassing six types (types I-VI) and over 30 subtypes (*4*). The CRISPR array consists of short "spacer" sequences derived from MGEs, interspersed between conserved direct repeats. Adjacent to CRISPR arrays are *cas* genes, which encode an effector complex of multiple Cas subunits (class 1) or a single-protein effector (class 2) (*4*). The long transcripts of CRISPR arrays are processed into small mature CRISPR RNA (crRNA) molecules, which direct the Cas effector to identify and cleave the invading nucleic acids. This process relies on a precise match between the crRNA spacer and the target "protospacer" sequence, found next to a specific 'protospacer adjacent motif' (PAM) (*5, 6*).

Recent research has uncovered the secondary function of Cas effectors in gene regulation, guided by a series of regulatory crRNA-like RNAs (crlRNAs) (*7-9*). Unlike traditional crRNAs, crlRNAs are encoded by solitary repeat units (SRUs) or mini-arrays and redirect Cas proteins to host promoter sequences for transcriptional repression. Importantly, the match between the crlRNA spacer sequence and the target protospacer is only partial, which allows target DNA binding without licensing cleavage (*7-9*). Our recent studies have systematically demonstrated the regulatory role of type I-B, I-E, I-F, and type V-A Cas effectors, which are directed by a crlRNA known as Cas-regulating (CreR) RNA (*10, 11*). CreR RNAs are typically encoded upstream of the Cas effector gene(s) and direct the Cas effector to repress its own promoter (see Fig. 1A for example). This autorepression has shown to reduce the risk of CRISPR autoimmunity while fine-tuning Cas expression to match the cellular abundance of endogenous crRNAs (which compete for Cas proteins with CreR), and up-regulating Cas expression when viral anti-CRISPR (Acr) proteins inactivate host Cas proteins *(10)*. Similarly, recent works have revealed that the majority of type II-A CRISPR-Cas systems encode a long isoform of the trans-activating crRNA (tracr-L) acting as a regulatory crlRNA, which re-directs Cas9 to auto-regulate its own expression, leading to a strong spike of Cas9 production when host Cas9 proteins are inhibited by Acr proteins (*12, 13*).

In addition, in some type I systems, CreR elements have shown to direct Cas proteins to transcriptionally inhibit a CreT toxin (CRISPR-repressed toxin) that is typically encoded next to the Cas effector genes (*8*). In these loci, CreR molecules are referred to as CreA (crRNA-resembling antitoxin) RNAs due to their antidote activity. These CRISPR-regulated toxin-antitoxin (CreTA) modules trigger cellular death/dormancy when *cas* genes are disrupted by transposable elements or when Cas proteins are compromised by Acr proteins encoded by MGEs. Indeed, we have recently demonstrated that CreTA systems safeguard CRISPR-Cas systems and expel Acr-encoding MGEs from the bacterial population, thus providing broad-spectrum anti-anti-CRISPR protection to CRISPR-Cas systems (*14*). This strategy is reminiscent of the immune guard hypothesis initially described in plants and increasingly recognized in prokaryotes, where the inhibition of one defense mechanism triggers the activation of another (*15-17*). However, little is known about how viruses overcome such multilayered defenses.

In a recent study, Shmakov *et al.* identified viral crRNA-like sequences resembling CreR elements in bacteria, which show partial complementarity to *cas* operon promoters (*9*). These findings suggest that these phage-encoded elements may interfere with host CRISPR-Cas expression, yet their functions remained enigmatic. In this study, we experimentally demonstrated that diverse viral crlRNAs can re-direct host Cas proteins to robustly suppress the expression of Cas proteins or CreT toxins, thus inhibiting the CRISPR-mediated adaptive immunity or the toxin-induced innate immunity, respectively. To distinguish these crlRNAs from their cellular counterparts (CreR and CreA), we refer to these viral Cas/CreT-repressing RNA anti-CRISPRs as Cracr RNAs, aligning with the nomenclature of Racrs (RNA anti-CRISPRs), recently demonstrated to sequester Cas proteins to form aberrant complexes (*18*). Remarkably, Cracr RNAs are frequently found stacked as CRISPR-like arrays in viruses to simultaneously block diverse CRISPR-Cas variants and/or their associated CreTAs. Moreover, we also uncovered the marked co-occurrence and functional synergy between type I-F Cracr RNAs and AcrIF24, an inhibitory protein that differentiates Cracrs from cellular crlRNAs/crRNAs based on their shorter spacer sequences. Therefore, our findings showcase the genetic diversity of viral anti-CRISPR elements and their mechanistic synergy, providing valuable insights for improving the efficacy of therapeutic phages and the safety of CRISPR-Cas tools.

Results

Two conserved Cracr RNAs encoded by *Pseudomonas aeruginosa* MGEs

To explore whether CreR-mediated Cas auto-repression is a strategy exploited by genetic parasites to suppress host Cas expression, we searched for MGE-encoded *creR* homologs across the genomes of the opportunistic pathogen *P. aeruginosa*. Bioinformatic screening of type I-F CRISPR-Cas loci across the *P. aeruginosa* genomes in the NCBI database revealed two conserved *creR* genes, *creRIF1* and *creRIF2*, located within the intergenic region between *cas2-3* and *csy1* (Fig. 1A). Notably, this intergenic region is only present in a fraction of *P. aeruginosa cas* operons and is absent in the well-studied PA14 I-F *cas* operon, likely explaining its late discovery. Blastn searches using *creRIF1* and *creRIF2* and manual exclusion of the hits within or nearby CRISPR-Cas loci revealed over 150 SRUs or mini-arrays that likely encode homologs of CreRIF1 and CreRIF2, which we referred to as candidate CracrIF1 and CracrIF2, respectively (Fig. 1B and Table S1). Notably, these

Cracr candidates are enriched on MGE sequences, primarily prophages and plasmids (Fig. 1B). Interestingly, while CracrIF1 RNAs prefer a 18-nt spacer-like sequence (ΨS), CracrIF2 prefer a 20-nt ΨS. We also noted high-level nucleotide conservation of the ΨS sequences, except for variations in nucleotides every 6th position (Fig. 1B), which are known not to base pair with the target DNA (*19, 20*). This marked sequence conservation indicates that *cracrIF1* or *cracrIF2* genes are mutationally constrained to maintain their base-paring potential to conserved DNA targets, suggesting their interaction with Cas proteins to carry out CreR-like functions.

Most of the identified *cracr* genes cluster with known Acr protein-coding genes, strongly suggesting their role in immune inhibition (Fig. 1B). While prophage IF *cracr* genes typically locate directly downstream of an *acrIF23-24* operon, in line with the findings of Shmakov et al (*9*). Plasmid-born *cracr* genes do not exhibit this pattern, though a co-occurring *acrIF1* gene was frequently observed (Fig. 1B). A systematic analysis of the genomic contexts of all available *acrIF24* genes revealed that nearly 88.76% of them are followed by *cracr* genes (fig. S1A), indicating a potential functional synergy between AcrIF24 and Cracr RNAs, as well as suggesting *acrIF24* may serve as a valuable marker to uncover further Cracr diversity. Facilitated by this marker, our systematic searches for *cracr* genes across taxa revealed diverse putative Cracr RNAs with 85 SRUs or mini-arrays that are carried by phages or MGEs from a series of non-*P. aeruginosa* bacteria (spanning 9 genera, and 7 orders of β-proteobacteria and γ-proteobacteria) (Table S2 and fig. S1B). These *cracr* genes typically share highly similar repeat sequences with a type I-F CRISPR array co-occurring within the same (or a closely-related) host genome, facilitating prediction of their ΨR and ΨS sequences. Notably, these *cracr* genes harbor different ΨS sequences, suggesting their ability to suppress a diversity of CRISPR-Cas loci. Accordingly, we predicted 8 CRISPR-Cas loci with their *cas* promoters likely being targeted by one of these *cracr* genes (Table S2). Altogether, our findings suggest that Cracr elements are widespread across diverse MGEs and are likely employed to silence host CRISPR-Cas immune functions.

CracrIF1 shows anti-CRISPR activity

The *Pseudomonas* phage vB_PaS_IME307 carries a *cracrIF1* gene (previously noticed by Shmakov *et al.* (*9*)) that is homologous to the *creRIF1* gene from *P. aeruginosa* NY5506, while the prophage in the *P. aeruginosa* strain P3-S8 contains a *cracrIF2* gene that is homologous to the *creRIF2* gene from *P. aeruginosa* strain Y010 (Fig. 1A). All the CRISPR repeat-like (ΨR) sequences of these Cracr candidates are highly similar to the consensus repeat of type I-F CRISPR arrays, except for the eight 3'-terminal nucleotides of their second ΨR (ΨR2) (fig. S2A). These sequences all contain internal palindromes indicative of a conserved RNA hairpin structure that is predicted to be recognized by the Csy4 endonuclease (Fig. 1B). Notably, the two *cracr* genes share 8 identical 3'-terminal nucleotides, which differ significantly from those of the two *creR* genes. In addition, the *cracr* genes have slightly shorter ΨS sequences (Fig. 1A). Therefore, it is likely that the ΨS and ΨR2 portions of the viral crlRNA genes (*cracr*) underwent adaptive evolution following their exaptation from the cellular genes (*creR*), while retaining the ability to interact specifically with host Cas proteins.

To functionally characterize the phage-encoded CracrIF1, we first confirmed its production from a plasmid in *P. aeruginosa* cells expressing the type I-F Cas system (fig. S2C). In PAO1 cells lacking a I-F CRISPR-Cas system, no small RNA products were detected by Northern blotting. However, the introduction of a plasmid expressing the PA14 Csy proteins (Csy1-Csy4) led to the detection of mature CracrIF1 RNAs, indicating specific binding and processing of CracrIF1 by host Cas proteins (fig. S2C). By constructing a chimeric *cas* operon (designated PA14-NY5506) composed of the complete set of PA14 *cas* genes and the NY5506 *cas* intergenic sequence including *creRIF1*, we also confirmed the production of mature CreRIF1 RNAs (fig. S2C). Notably, the CracrIF1 RNAs were observed to be slightly smaller than host CreRIF1 RNAs, consistent with their differing ΨS sizes (18-nt and 20-nt, respectively). Despite this small difference, the ΨS sequences of CracrIF1 and CreRIF1 share 17 identical nucleotides, enabling almost perfect base pairing (except the 6th nucleotide) with a target sequence upstream of the NY5506 *csy* operon (Fig. 2A). The presence of a canonical type I-F PAM, i.e., 5'-CC-3' further indicated that CracrIF1 and CreRIF1 both have the potential to direct the Csy complex to bind to this target site. Together, these data indicate that both CracrIF1 and CreRIF1 are effectively matured like endogenous crRNAs by Csy4 and contain a ΨS predicted to bind upstream of the *csy* operon.

To investigate whether the predicted binding of CreRIF1 and CracrIF1 to their target site impacts Cas expression, we first mapped the location of the transcription start site (TSS) of the NY5506 *csy* operon through 5' RACE analysis (fig. S3A) and predicted its -35 and -10 promoter elements (Fig. 2A). Interestingly, the *csy* transcripts have an unusually long 5' untranslated region (5'-UTR), later discovered to produce an RNA toxin (see below). To evaluate the potential *cys*-silencing effect of CreRIF1 and CracrIF1, we constructed a fluorescent mCherry reporter under the control of the *csy* promoter (P_{csy}) and confirmed its TSS through primer extension (consistent to the results of 5' RACE; fig. S3B). By measuring the fluorescence signal in PAO1 cell culture expressing the PA14 Csy proteins along with CracrIF1 or CreRIF1, we observed that CracrIF1 and CreRIF1 reduced the strength of P_{csy} by a factor of 14 and 21, respectively (Fig. 2B). Importantly, when we mutated three ΨS nucleotides (indicated in Fig. 1A) of either RNA regulator to disrupt its complementarity with P_{csy}, the inhibitory effects were no longer observed (Fig. 1C). Therefore, the phage-encoded CracrIF1 redirects host Cys complexes to specifically silence the *cys* operon, likely providing phages with a means to immunosuppress host cells.

To evaluate the anti-CRISPR effects of CracrIF1 in the context of infection, we isolated a siphophage infecting PAO1, ΦW8-1 (fig. S4A), and designed a crRNA targeting its tail tape measure protein gene (fig. S4B). In PAO1 cells containing the chimeric PA14-NY5506 *cas* operon, the phage-targeting crRNA resulted in a reduction of 3-4 logs in plaque forming units (PFUs) compared to a non-targeting control (Fig. 2C). However, the expression of CracrIF1 RNA rescued phage infectivity to the level of the non-targeting control, demonstrating its robust anti-CRISPR activity. Indeed, mutating the ΨS sequence (nucleotides 1-3; seed) of CracrIF1 completely reverted its immunosuppressive activity (Fig. 2C), underscoring the importance of base pairing with the P_{csy} target. Quantitative PCR further confirmed that CracrIF1 markedly reduced *csy* transcripts level (by approximately 75%; Fig. 2D). Notably, the target-binding requirement distinguishes Cracrs

212 from the recently reported Racr RNAs, which lack a ΨS and rely on the interaction between
213 their repeat portions and Cas proteins. We conclude that CracrIF1 transcriptionally inhibits
214 Cas proteins by mimicking the RNA-guided auto-regulatory function of host CreR RNAs,
215 presenting a distinct RNA-based anti-CRISPR mechanism exploited by phages.
216
217 **CracrIF2 does not show anti-CRISPR activity**
218 We then aimed to functionally characterize CracrIF2, which exhibits a strong genetic
219 association with *acr* genes, including *acrIF24* and *cracrIF1* (Fig. 1B). The ΨS sequences
220 of CracrIF2 and CreRIF2 share 17 identical nucleotides, forming extensive base pairings
221 to a sequence upstream of the Y010 *csy* operon. This predicted target is adjacent to a 5'-
222 CC-3' PAM sequence and includes mismatches at positions 6 and 12, which do not affect
223 target DNA recognition (Fig. 3A). Therefore, we posited that CracrIF2 exhibits anti-
224 CRISPR activity against the Y010 CRISPR-Cas system. However, we were unable to
225 obtain sufficient immune targeting against ΦW8-1 by the Y010 system in PAO1. Therefore,
226 we engineered a chimeric *cas* operon (designated as PA14-Y010) that comprises the
227 closely-related PA14 *cas* genes and the Y010 IGR between *cas2-3* and *csy1* (containing
228 *creRIF2* and its target). Unexpectedly, while this chimeric operon conferred robust
229 immunity against phage ΦW8-1 in PAO1 cells, expression of CracrIF2 RNAs did not
230 provide the phage with a replicative advantage, indicating the inability of CracrIF2 to
231 suppress immunity (Fig. 3B). To investigate the reasons for this lack of inhibitory activity,
232 we investigated the production and maturation of CracrIF2. Northern blotting revealed that
233 CracrIF2 RNAs (as well as CreRIF2 RNAs) were effectively matured in PAO1 cells
234 expressing the PA14 Csy proteins (fig. S5). Processing was further confirmed via small
235 RNA sequencing, which showed the characteristic 5' and 3' handles of endogenous
236 crRNAs (fig. S5D). Thus, we concluded that the failure of CrarIF2 to inhibit CRISPR
237 immunity could not be attributed to inappropriate Cracr RNA maturation.
238
239 To gain mechanistic insights into the lack of anti-CRISPR activity by CracrIF2, we
240 experimentally identified the promoter of the Y010 *csy* operon by mapping its TSS via 5'
241 RACE (fig. S6A). Surprisingly, we identified two TSS in this region, each preceded by an
242 evident promoter sequence (labeled in Fig. 3A). Interestingly, CracrIF2 targets the
243 promoter farther from *cys1*, potentially silencing a short cryptic gene in the intergenic
244 region before the *csy* operon, which may explain its lack of anti-CRISPR activity. Notably,
245 our previous research has demonstrated that certain CreR-like elements are part of minimal
246 TA systems, which encode crRNA-resembling antitoxins (CreA) that complex with Cas
247 proteins and guide them to inhibit the transcription of a small RNA toxin gene (designated
248 *creT* for CRISPR-repressed toxin) located within the intergenic regions between *cas* genes
249 (*8, 21*). Motivated by the architectural resemblance of CreA loci with the site targeted by
250 CracrIF2, we carefully examined the 5' UTR of the long *csy* transcripts. We noticed a mini-
251 ORF (of 15 nt) preceded by a putative Shine-Dalgarno (SD) sequence and followed by a
252 hairpin structure (Fig. 3A), reminiscent of the small RNA toxins we previously discovered
253 that sequester rare transfer RNAs using two or more consecutive rare codons (*8, 21*).
254 Despite failing to identify any rare codons within the mini-ORF, we used an inducible *tac*
255 promoter to express a series of differently truncated RNA transcripts and confirmed that
256 the SD sequence, mini-ORF, and hairpin structure cause toxicity in PA14 cells (fig. S7, A
257 and B). Through point mutations, we further confirmed the simultaneous requirement of

258 the three elements for toxicity (Fig. 3C). Therefore, Y010 *csy* transcription can be driven
259 by both a promoter shared with a small RNA toxin (likely suppressed by CracrIF2 and
260 CreRIF2), and also by an independent promoter closer to *csy1*, explaining why CracrIF2
261 fails to inhibit CRISPR immunity. For clarity, we designate the toxin as CreT and refer to
262 CreRIF2 as CreA hereafter.
263
264 **CracrIF2 transcriptionally inhibits a unique RNA toxin**
265 To understand how the identified rare-codon-lacking CreT elicits toxicity, we deleted or
266 inserted one or more nucleotides following its ATG start codon. Remarkably, toxicity
267 persisted only when three nucleotides were deleted (fig. S7C). This underscores the
268 important role of the downstream codons, which, interestingly, include two consecutive
269 proline codons (CCT and CCG) except the stop codon (Fig. 3A). Subsequently, we
270 constructed a series of variants with these two proline codons substituted by other
271 synonymous or non-synonymous codons (Fig. 3D). Toxicity was maintained only when
272 one or both proline codons were synonymously altered, indicating two consecutive proline
273 codons at this position are critical for toxicity. Previous studies have shown that during
274 protein translation, peptide bond formation is especially slow with proline, and two
275 continuous proline codons can cause ribosomal stalling (*22, 23*). Therefore, we propose
276 that this CreT is a novel small RNA toxin that exploits two highly and consecutively
277 translated proline codons, presumably leading to severe ribosome stalling and eventual
278 starvation.
279
280 The location of the target of CracrIF2 and CreA (CreRIF2) suggests that these crlRNAs
281 may inhibit the promoter of *creT* (P_{creT}) rather than P_{csy} of Y010. To explore this hypothesis,
282 we constructed fluorescent reporters by linking the P_{creT} DNA to *mCherry* and validated its
283 TSS through primer extension (consistent to the results of 5' RACE; fig. S6B). By
284 measuring the fluorescence signal, we demonstrated that both CracrIF2 and CreA reduced
285 the activity of P_{creT} by a factor of 34 and 30, respectively, in the presence of PA14 Csy
286 proteins (Fig. 3E). Complementary mutations further confirmed that their inhibitory effects
287 relied on critical base-pairings to the target promoter (Fig. 3E). We also evaluated the *P.*
288 *aeruginosa* CreTA module in *E. coli* cells. Introduction of a plasmid carrying the Y010
289 *creT-csy* operon and an IPTG-inducible *creA* gene into MG1655 cells resulted in severe
290 growth defects under non-inducing conditions but not under inducing conditions (Fig. 3F),
291 which demonstrated that the toxicity of the *P. aeruginosa* CreT in *E. coli* cells and the
292 crucial antidote role of CreA. Notably, when another plasmid expressing CracrIF2 was also
293 introduced into these cells, growth defects were not observed under either condition,
294 highlighting its robust anti-CreTA activity (Fig. 3F). Taken together, our results
295 demonstrate that CracrIF2 mimics the CreA to transcriptionally inhibit the CreT RNA toxin.
296
297 **CracrIF2 subverts the innate immunity induced by CreTA**
298 The targeting of CreTA by CracrIF2 raises intriguing questions about the evolutionary
299 drivers of these inhibitory elements. Our recent study revealed that CreT toxins, which are
300 normally suppressed by CRISPR-Cas systems, are activated by a variety of Acr proteins to
301 induce abortive infection, ultimately killing infected cells to prevent further viral spread in
302 the population (*14*). We have shown that this innate immune process does not rely on
303 CRISPR targeting and can expel Acr-encoding MGEs from bacterial populations, thus

304 providing a broad-spectrum anti-anti-CRISPR protection for CRISPR-Cas. Therefore, we
305 reasoned that phages may counteract CreTA-mediated anti-Acr defense through CracrIF2
306 deployment. To experimentally test this, we introduced the entire Y010 *cas* operon,
307 including its *creTA* genes, into PAO1 cells and then expressed AcrIF24 (frequently linked
308 with *cracr* genes) using the BAD promoter (P_{BAD}) (Fig. 4A). As expected, PAO1 cells
309 exhibited growth defects when AcrIF24 was expressed through arabinose induction, but
310 not when its expression was repressed with glucose, indicating that the *P. aeruginosa* CreT
311 was activated by AcrIF24 expression. Consistently, growth defects were no longer
312 observed when *creT* was mutated (Fig. 4A). However, growth defects were alleviated when
313 CracrIF2 RNAs were expressed *in trans* from another plasmid, consistent with its anti-
314 CreTA function (Fig. 4A). A similar rescuing effect was observed when *cracrIF2* was
315 placed downstream of *acrIF24* to reproduce their natural genetic arrangement in phage
316 genomes (fig. S7D). Our results demonstrate that CracrIF2 counteracts the anti-anti-
317 CRISPR effect of CreTA against AcrIF24 protein deployment, thereby representing an
318 unprecedented RNA-based anti-anti-anti-CRISPR mechanism.
319
320 To further explore the anti-CreTA effect of CracrIF2 at the population level, we engineered
321 two reporter plasmids, one containing *gfp* (pGFP) and the other containing *mCherry* (pMC),
322 and introduced them in a 1:1 ratio to *P. aeruginosa* PAO1 cells expressing the PA14-Y010
323 *cas* operon (Fig. 4B). In our experiments, pMC was designed to encode no anti-CRISPR
324 factors (negative control), the AcrIF24 protein alone, or both the AcrIF24 protein and the
325 CracrIF2 RNA. By monitoring the green and red fluorescence, we showed that when only
326 AcrIF24 was induced, pMC was swiftly eliminated from the *P. aeruginosa* bacterial
327 populations (Fig. 4B). These results demonstrate a herd immunity process mediated by the
328 Y010 CreTA module. However, the presence of CracrIF2 RNAs disrupted this herd
329 immunity protection, as evidenced by the lack of pMC elimination in the bacterial
330 population (Fig. 4B). Altogether, our data underscores that the CracrIF2 RNA suppresses
331 the CreTA-mediated herd immunity response against phage Acr proteins.
332
333 **AcrIF24 differentiates CreA and Cracr by spacer size**
334 Previous studies have revealed that AcrIF24 inhibits CRISPR immunity by directly binding
335 to Csy-crRNA complexes, preventing interaction with their DNA targets (*24*). Since Cracrs
336 guide the Csy complex to hybridize with host immune promoter DNA targets, this raises
337 questions about how AcrIF24 does not negatively affect the activity of Cracrs. Surprisingly,
338 Cracrs show a strong genetic association with AcrIF24 (Fig. 1B), suggesting that these
339 elements either synergize or are at least not functionally incompatible. To explore the
340 potential impact of AcrIF24 on the RNA-guiding activity of CracrIF2 and CreA, we
341 established an *mCherry*-based reporter assay in PAO1 cells expressing PA14 Csy proteins
342 (Fig. 5A). Remarkably, while the ability of CreA to repress P_{creT} was significantly impaired
343 by AcrIF24 (repression fold decreased from 30.6-fold to 1.88-fold; P =9.25e-07), the
344 regulatory activity of CracrIF2 was almost unaffected (P = 0.08). By excluding Cracr and
345 CreA components from the assay, we confirmed that AcrIF24 (which can also act as an
346 Acr-associated transcriptional regulator (24)) does not independently regulate P_{csy} (Fig. 5A).
347 These results reinforce the suspicion that AcrIF24 can discriminate between CracrIF2-
348 guided and CreA-guided Csy complexes.
349

By comparing the sequences of the *cracrIF2* and *creA* elements, we hypothesized that discrimination by AcrIF24 could rely on the differing nucleotides in their ΨR sequences, their different ΨS sizes, or a combination of both (Fig. 5B). To explore the importance of the ΨR sequence identity, we substituted the ΨR sequences of *cracrIF2* with those of *creA* (Fig. 5B). However, the resulting mutant (*cracrIF2*-sub) was still able to effectively repress the targeted P_{creT} in the presence of AcrIF24 (Fig. 5C), thus ruling out a mechanism dependent on the ΨR sequence composition. Next, we extended the ΨS sequence of *cracrIF2* from 21 nt to 26 nt, matching the size of the ΨS in *creA* (Fig. 5B). In this experiment, Csy complexes guided by the ΨS-extended *cracrIF2* became significantly susceptible to AcrIF24 (Fig. 5C), suggesting that the ΨS size is mechanistically important for AcrIF24 to distinguish between CracrIF2-guided and CreA-guided Csy complexes. Indeed, in a survey of all identified type I-F *cracr* genes and their *creA* or *creR* counterparts (listed in Table S2), we noticed a significant difference in their ΨS sizes (P = 6.23E-08) (Fig. 5D). While Cracr RNAs prefer a ΨS size between 18-21 nt, CreA/CreR RNAs usually favor a ΨS sequence of 24-26 nt.

To further investigate the role of ΨS in AcrIF24 discrimination, we created a series of CracrIF2 derivatives with ΨS sequence lengths ranging from 18 nt to 26 nt. Our observations revealed that the regulatory effect became susceptible to AcrIF24 inhibition only when the spacer size exceeded 22 nt (Fig. 5E). Consistently, the regulatory effects of CracrIF1 (18 nt) and CreRIF1 (20 nt) on the NY5506 *csy* promoter were both resistant to AcrIF24 (fig. S8). This suggests that CreRIF1-mediated regulation of Cas proteins—and likely the CreT RNA toxin—does not sense the presence of this specific anti-CRISPR protein. Taken together, our results reveal a unique discriminatory mechanism by AcrIF24 to distinguish between host and phage-derived crlRNAs, depending on slight differences in their ΨS lengths.

AcrIF24 cannot bind Csy-Cracr complexes with fewer Csy3 subunits

The length of the crRNA has structural implications for type I interference complexes, determining the number of Csy3 subunits that assemble to form the backbone. Therefore, we hypothesized that the different spacer sizes of the crRNA, CreA, and Cracr elements—as confirmed via Northern blotting (fig. S5, A and B)—likely impact the number of Csy3 subunits in the resulting Csy complexes. To explore this, we purified the Csy complexes assembled with different backbone RNAs through affinity purification of His_6-Csy1. During size-exclusion chromatography (SEC), the elution peak of the Csy-crRNA complex appeared first, immediately followed by the Csy-CreA complex, with the Csy-CracrIF2 elution peak appearing last and revealing a flatter shape (Fig. 6A). This indicated a smaller and inconsistent ratio of Csy3 subunits in the Csy-CracrIF2 complex, in line with its shorter spacer. In agreement, native PAGE (polyacrylamide gel electrophoresis) analysis of the Csy-CracrIF2 complexes showed diffused bands, indicating the presence of a mixture of complexes with varying Csy3 ratios (fig. S5C). Furthermore, through SDS-PAGE, we confirmed that the Csy-CracrIF2 complex contained fewer Csy3 subunits compared to the complexes containing crRNA or CreA (Fig. 6B).

A previous study uncovered that AcrIF24 binds to the Csy-crRNA complex via its extensive interaction with five Csy3 subunits (*24*). These results led us to speculate that AcrIF24 may

be unable to bind to the Csy-CracrIF2 complex which has fewer Csy3 subunits. To investigate this, we performed pull-down assays using GST-labeled AcrIF24 to capture the different Csy complexes containing crRNA, CreA, or CracrIF2. Our results showed that Csy-crRNA and Csy-CreA complexes were effectively pulled down, while only a minimal amount of Csy-CracrIF2 complexes were captured (Fig. 6C). This suggests that AcrIF24 exhibits significantly lower binding affinity to Csy-CracrIF2 compared to Csy-crRNA and Csy-CreA complexes. Additionally, we investigated the target DNA binding specificity of different Csy complexes in the presence or absence of AcrIF24. Remarkably, AcrIF24 promoted Csy-crRNA and Csy-CreA to bind to non-target DNA, while Csy-CracrIF2 continued to specifically associate with target DNA regardless of the presence of AcrIF24 during the competition assay (Fig. 6D).

Using cryogenic electron microscopy (Cryo-EM), we sought to shed light on the structural and mechanistic nuances of the Csy complexes assembling with different RNA guides (Fig. 6E). Notably, the Csy-crRNA and Csy-CreA complexes contained six and five Csy3 subunits, respectively, while the Csy-Cracr complex primarily featured four Csy3 subunits. By comparing the structures to the previously reported Csy-Acr24 complex, we observed that the lack of Csy3.1 and Csy3.2, but not the lack of only Csy3.1, significantly reduced the interface between the Csy complex and AcrIF24 (Fig. 6F). Therefore, we conclude that the functional compatibility between CracrIF2 to AcrIF24 is a result of its shorter spacer size, which leads to the absence of two Csy3 subunits essential for AcrIF24 binding to the Csy complex. Together, these structural analyses underscore the unprecedented co-evolution of protein and RNA anti-CRISPRs, resulting in their functional synergy to effectively counter both adaptive and innate immune functions in bacteria.

A Cracr array inhibits both adaptive and innate immunity

Interestingly, eight *P. aeruginosa* prophages and two closely-related plasmids were found to carry a combined structure featuring both *cracrIF1* and *cracrIF2* ΨS sequences (thus referred to as *cracrIF1/2*) (Fig. 1B). This stacked configuration resembles a two-spacer CRISPR array, which we hereafter refer to as Cracr array. By comparing the ΨR sequences of the Cracr array with those of the individual *cracrIF1* and *cracrIF2* genes (Fig. 7A), we observed significant homology and similar nucleotide variations in the first (ΨR1) and second (ΨR2) repeat sequences. Notably, ΨR2 of the Cracr array retains 8 conserved 3'-terminal nucleotides (5'-CTAAGAAA-3'), essential for generating a typical 8-nt 5' handle for its CracrIF2 RNA products. In contrast, the last ΨR (ΨR3) of the Cracr array shares 8 identical terminal nucleotides (5'-AGAAAGGC-3') with the ΨR2 (also the last ΨR) of *cracrIF1* and *cracrIF2* (Fig. 7A). Importantly, the starting nucleotides (5'-TATGA-3') of ΨR3 are significantly different from those of other ΨR sequences, and notably, the second ΨS of the Cracr array (18-nt) is 3 nucleotides shorter than the corresponding ΨS from standalone *cracrIF2* genes (21-nt) (Fig. 7A). Therefore, it appears that the *cracrIF1/2* Cracr array did not originate from a direct recombination event between *cracrIF1* and *cracrIF2*, but rather likely emerged from an integration event within the ΨR2 sequence of *cracrIF1* that is unrelated to standalone *cracrIF2* genes.

We next aimed to explore the potential multiplexed functionality of the identified Cracr array. Through Northern blotting, we confirmed that the Cracr array indeed produced both

442 CracrIF1 and CracrIF2 RNAs in PAO1 cells expressing the PA14 Csy proteins (fig. S9A).
443 We then examined the potential anti-CRISPR function of the Cracr array by introducing it
444 into PAO1 cells that contained a phage-targeting mini-CRISPR and the chimeric *cas* operon
445 PA14-NY5506 (Fig. 7B). Upon infection by phage ΦW8-1, we observed that the Cracr
446 array robustly suppressed the immune targeting ability of PA14-NY5506, with its effect
447 relying on the seed nucleotides of its first rather than its second ΨS. Next, we introduced
448 the Cracr array along with an inducible *acrIF24* gene into PAO1 cells that contained the
449 Y010 *cas* operon (Fig. 7C). In this setup, when AcrIF24 was expressed, the Cracr array
450 completely suppressed the anti-anti-CRISPR response (arresting cell growth) mediated by
451 the Y010 *creTA* genes, and this suppression relied on its second rather than its first ΨS.
452 Therefore, the Cracr array exhibited both anti-CRISPR and anti-anti-anti-CRISPR
453 activities, which cooperatively confronted the adaptive immunity and innate immunity
454 pathways mediated by the host CRISPR-Cas and CreTA elements.
455
456 Among the non-*P. aeruginosa cracr* genes, we were surprised to observe that a
457 considerable fraction (35 out of 85) evolved arrays of at least two ΨS sequences, with ten
458 arrays and two arrays even containing 3 and 4 different ΨS sequences, respectively (Table
459 S2). Specifically, we investigated the three-spacer Cracr array from the *Burkholderia*
460 *gladioli* strain BCC1711, and two related dual-spacer arrays from the *B. gladioli* strains
461 BCC1700 and BCC1864 (fig. S9B). The two ΨS sequences of BCC1700 closely resemble
462 the second and third ΨS of BCC1711, while the two ΨS sequences of BCC1864 are almost
463 identical to the first and third ΨS of BCC1711. Together, our findings suggest that
464 assembling individual *cracr* genes into a multifunctional anti-defense array is likely a
465 common strategy employed by different MGEs to confront different CRISPR-Cas variants
466 and their associated CreTA modules.
467
468 ***Salmonella* MGEs use Cracrs to silence host I-E CRISPR-Cas**
469 We then wondered if Cracr elements could also target other CRISPR-Cas systems beyond
470 the studied type I-F. For this purpose, we searched for putative *cracr* genes targeting I-E
471 CRISPR-Cas by performing bioinformatic searches across MGE genomes with previously
472 identified type I-E *creR* genes as querries. Using this approach, we discovered three
473 putative Cracr RNAs encoded by *S. enterica* MGEs, including prophages and plasmids,
474 which we named CracrIE1, CracrIE2, and CracrIE3 (fig. S10A). In the *S. enterica* subsp.
475 salamae serovar 56:b:[1,5] strain SA20053897, one prophage contains a two-spacer array
476 (namely *cracrIE1/2*) encoding CracrIE1 and CracrIE2, while another prophage contains a
477 single-spacer gene (*cracrIE2*) encoding CracrIE2. In the *S. enterica* subsp. diarizonae
478 strain CFSAN030538, a plasmid carries a dual-spacer array (*cracrIE3/2*) encoding
479 CracrIE3 and CracrIE2. Therefore, *S. enterica* MGEs appear to also have developed
480 individual and multiplexed Cracr elements.
481
482 Prediction of their potential regulatory targets revealed that the three CracrIE RNAs each
483 share a similar ΨS sequence with a *creR* gene (designated *creRIE1*, *creRIE2*, or *creRIE3*),
484 and each shared ΨS sequence matches a target sequence located between the corresponding
485 *creR* and the downstream *casA* gene (fig. S10B). Note that we suggest referring to these
486 cellular crlRNA genes as *creR,* rather than *creA,* until the cognate *creT* pair gene is
487 identified. To explore its putative transcriptional repression activity, we introduced a

plasmid containing the *cracrIE1/2* array into *E. coli* MG1655 cells, along with a second plasmid expressing GFP and a third plasmid over-expressing the *E. coli* Cascade proteins (fig. S10C). When GFP expression was driven by the putative promoter sequence targeted by *creRIE1* (from the *S. enterica* strain FDAARGOS_717), the fluorescence signal was significantly silenced by *cracrIE1/2* (fig. S10D), which was dependent on the integrity of the first ΨS. Similarly, when GFP expression was controlled by the putative promoter sequence targeted by *creRIE2* (from strain CFSAN001011), fluorescence was suppressed by *cracrIE1/2,* unless its second ΨS was mutated (fig. S10E). Our results demonstrate that the *cracrIE1/2* array can transcriptionally target two distinct type I-E CRISPR-Cas variants. However, the exact physiological activity of this array—whether it acts as an anti-CRISPR or an anti-anti-anti-CRISPR—requires further investigation.

Discussion

Disabling host defense systems is a crucial strategy employed by genetic invaders to ensure their survival and proliferation. Phages and plasmids have evolved various mechanisms to counteract bacterial CRISPR-Cas immunity, exemplified by over one hundred identified Acr protein families (*25, 26*) and the recent discovery of Racrs (*18*). However, the mechanisms allowing phages to evade the typically multilayered defenses of bacteria remain poorly understood. In this study, we introduce a distinct category of anti-CRISPR RNAs, known as Cracr RNAs, which suppress the expression of Cas proteins or a CRISPR-regulated toxin (CreT) by mimicking the regulatory crRNA-like RNAs (crlRNAs) of CRISPR-Cas.

Our previous work has shown that CRISPR-Cas systems use regulatory crlRNAs, like CreR and CreA, to modulate adaptive and herd immunity, respectively. CreR directs Cas proteins to target their own promoter and boosts Cas protein levels in the presence of Acr inhibitors (*10*). CreA directs Cas proteins to inhibit the promoter of the CreT toxin and elicits abortive infection when Acr proteins inhibit the Cas surveillance complex, ultimately providing herd immunity against Acr-encoding MGEs (*14*). CreTA elements thereby provide an anti-anti-CRISPR layer for CRISPR immunity. Remarkably, this study further unveils another layer of complexity to the MGE-CRISPR arms race, demonstrating how viral crlRNAs mimic cellular RNAs to counteract both the adaptive and herd immunity mediated by CRISPR-Cas systems (Fig. 7D). Viral mimics of CreR RNAs, like CracrIF1, exhibit anti-CRISPR function by robustly inhibiting Cas expression. Conversely, mimics of CreA RNAs, such as CracrIF2, can suppress CreT, undermining herd immunity and showing an unprecedented anti-anti-anti-CRISPR activity.

We further show that multiple Cracr RNAs, capable of inhibiting both adaptive defense and innate herd immunity, are frequently stacked within the same transcriptional unit. The structural resemblance between viral Cracr arrays and bacterial CRISPR arrays underscores the multiplexing potentials of both defensive and anti-defensive small RNAs. Such multivalent properties of Cracr arrays may play a crucial role as a phage bet-hedging strategy to overcome CRISPR-Cas systems in different hosts or to cooperatively thwart multilayered defenses. In addition, Cracr RNAs often work in tandem with protein anti-CRISPRs, at least for type I-F, where CracrIF RNAs are genetically linked to proteins like AcrIF23 and AcrIF24. While AcrIF23 disrupts the Cas2-3 nuclease, AcrIF24 inhibits the

binding of the Csy complex to DNA targets (*24*). Given that target promoter binding is crucial for Cracr RNA function, the co-locaiton of Cracrs with AcrIF24 was initially paradoxical. However, we discovered that Csy-Cracr complexes can remarkably evade AcrIF24 inhibition by utilizing shorter spacer sequences, leading to the absence of two Csy3 subunits necessary for AcrIF24 binding. (Fig. 6, E and F). These results showcase the delicate co-evolution of RNA and protein anti-CRISPR strategies. Furthermore, the identification of CRISPR-safeguarding CreTA elements, as well as the common genomic clustering of various defense genes into so-called "defense islands", indicate that defense systems may collaborate or protect each other, offering a multi-layered defense strategy (*27*). In contrast, our discovery of viral Cracrs, their clustering into anti-defense Cracr arrays, and the elegant functional synergy with anti-CRISPR proteins, strongly suggests that phages in parallel counter-evolve multi-layered anti-defense strategies. This intricate co-evolutionary dance between phages and bacteria showcases an ongoing arms race for survival, with each side developing sophisticated strategies to outmaneuver the other.

In summary, our findings uncover how phages hijack the RNA-guided properties of Cas effectors, developing RNA-based anti-CRISPRs or anti-anti-anti-CRISPRs. These elements can functionally cooperate with each other or with Acr proteins to effectively inhibit the adaptive and/or herd immune capabilities of different CRISPR-Cas variants. Together, these discoveries highlight the genetic and mechanistic diversity of viral anti-CRISPR elements and offer valuable insights for developing CRISPR-resistant therapeutic phages and more effective payload delivery vectors.

Acknowledgments
This work was supported by the Strategic Priority Research Program of the Chinese Academy of Sciences [XDB0830000], the National Key Research and Development Program of China [2022YFC3401500 and 2022YFC2104800], the National Natural Science Foundation of China [32150020, 32270092, 32370090, 32200057, and 32022003], the Lundbeck Fonden grant [R347-2020-2346], the research grant from VILLUM FONDEN [VIL60763], and the Youth Innovation Promotion Association of CAS [2020090].

Author contributions
M. L. conceived and supervised the project with valuable suggestions from R.P.-R., M.L, R.P.-R., Y.F., C.L., R.W., H.Z., and W.W. designed the experiments. J.Y., C.L., M.R.-M., and R.P.-R. performed the bioinformatics analyses and predicted Cracr genes. C. L. and R.W. generated strains and plasmids. C.L. performed phage infection assays. C.L. and R.W. conducted the efficiency of plaque assays and liquid culture growth assays. C.L., R.W. and J.D. performed the fluorescence measurement. C.L. J.X and S.X. performed RNA-seq and primer extension assays. C.L. conducted the 5' RACE assays. H.Z, T.Z., and Q.X. provided the phage and genome sequences. Z.L, X.D., and L.G. conducted protein purification. Y.F. and W.W. resolved proteins Cryo-EM structure. Z.L performed EMSA and protein pull-down assays. F.C. performed RT-qPCR. M.L., C.L., R.W., Z.L., and W.W. analyzed data. M.L. prepared the original draft. M. L., R.P.-R., and Y. F. finalized the manuscript with input from all authors.

Competing interests: The authors declare no competing interests.

Data and code availability: Data are publicly available. The atomic coordinates for the cryo-EM structures of type I-F cascade complexed with crRNA (PDB 9JPH), CreA (PDB 9JPG) and CracrIF2 (PDB 9JPF) were deposited to the PDB (www.rcsb.org). The cryo-EM density maps reported in this study for the type I-F cascade complexed with crRNA (EMD-61700), CreA (EMD-61699) and CracrIF2 (EMD-61698) were deposited to the EM Data Bank. The raw data for the RNAseq experiments in fig. S5D were deposited to the NCBI with the BioProject accession number PRJNA1173583. All additional data reported in this paper will be shared by the lead contact upon request. This paper does not report original code.

Supplementary Materials

Materials and Methods

Figs. S1 to S10

Tables S1 to S4

Figures

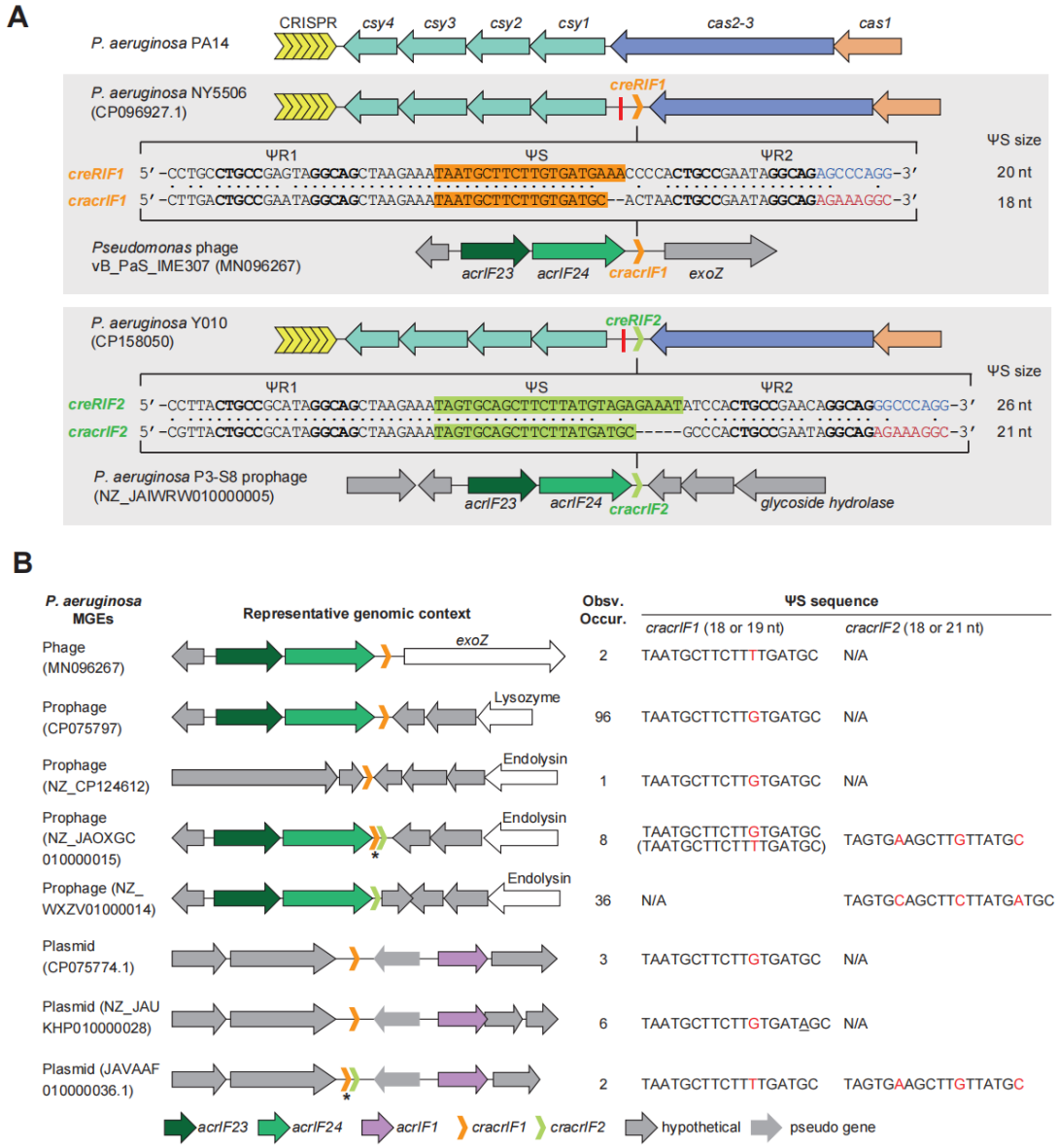

Fig. 1. Two conserved *P. aeruginosa cracr* genes and their *creR* homologs.
(**A**) Illustration showing the homology between representative *cracrIF1* or *cracrIF2* and their *creR* homologs. Dots indicate the identical nucleotides. Eight differing terminal nucleotides are highlighted in red (*cracr*) or blue (*creR*). Palindromic nucleotides within each ΨR sequence are bolded. The size of ΨS is provided for each crlRNA gene. The red vertical bar represents the target sequence of *cracr* and *creR*. The well characterized PA14 *cas* operon is also included for comparison. (**B**) Occurrences of *cracrIF1* and *cracrIF2* genes in *P. aeruginosa* MGEs and their varied genomic contexts. Single ΨS nucleotides displaying polymorphism are highlighted in red. An asterisk (*) denotes a CRISPR-like array encoding both CracrIF1 and CracrIF2 RNAs.

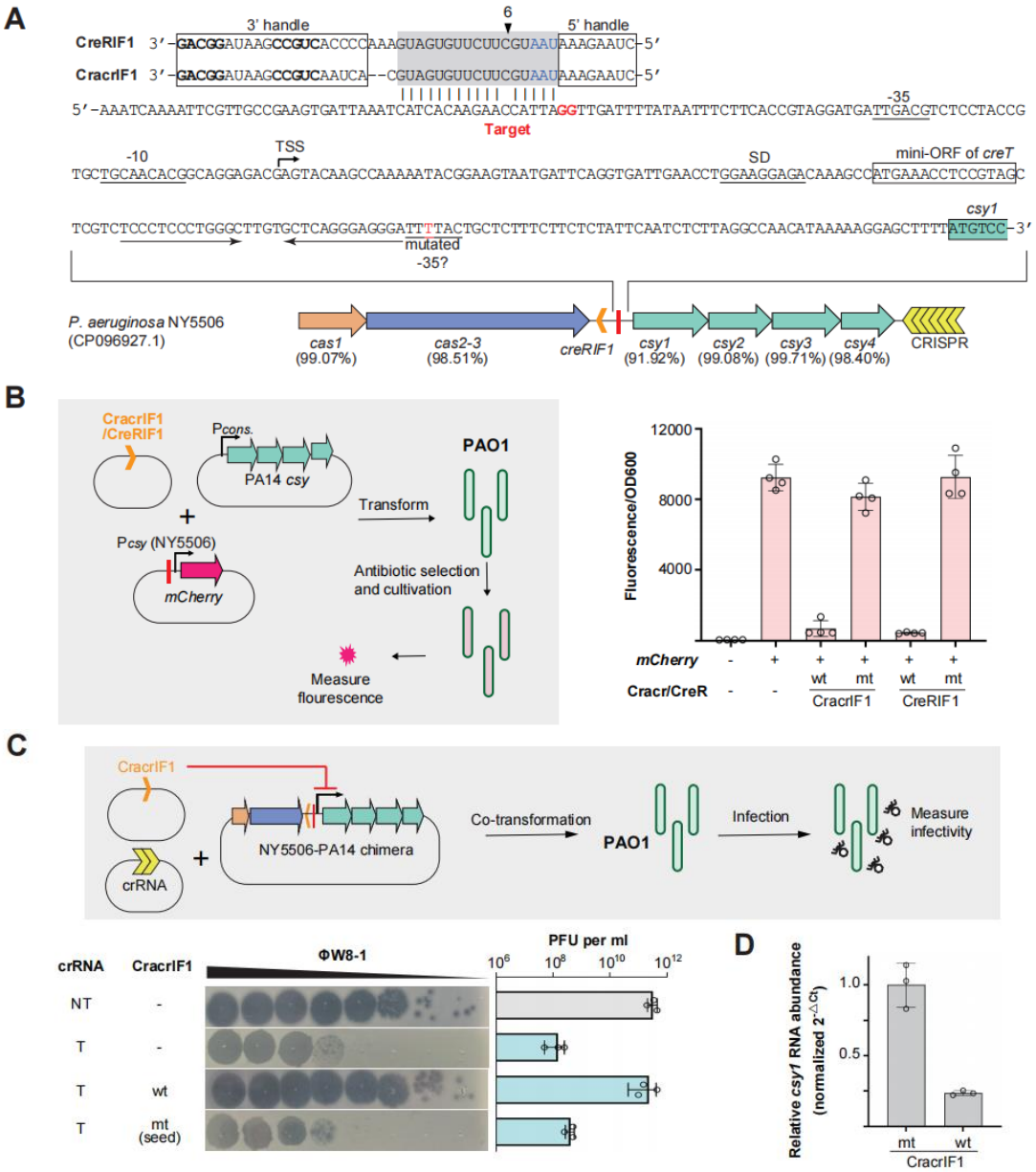

Fig. 2. CracrIF1 displays anti-CRISPR activity against the NY5506 CRISPR-Cas system. (**A**) Illustration showing the targeting potential of CracrIF1 and CreRIF1 to the *csy* promoter (P_{csy}) of *P. aeruginosa* NY5506. Nucleotides complementary to PAM are highlighted in red. Mismatch at position 6 (respective to PAM) is indicated. The identical ΨS nucleotides shared by CracrIF1 and CreRIF1 are shaded in gray. Blue nucleotides were mutated in panels **B** and **C**. Nucleotides of 5' and 3' handles are framed. Palindromic nucleotides within 3' handle are in bold. TSS was determined by 5' RACE (see fig. S3). Functional elements of a cryptic CreT RNA toxin, including an SD sequence, a mini-ORF, and a pair of inverted repeats (labeled with two convergent arrows), are also indicated. A red thymine (T) likely has inactivated a -35 element (underlined). Sequence similarities shared by PA14 and NY5506 Cas proteins are noted. (**B**) Fluorescence intensity from PAO1 cells with an *mCherry* gene under the control of the NY5506 P_{csy}. Three seed nucleotides (highlighted in blue in panel **A**) of CracrIF1 and CreRIF1 were mutated (mt). wt, wild-type. Error bars, mean±s.d. (n=4). (**C**) Plaque forming units (PFU) of ΦW8-1 infecting PAO1 cells with a phage-targeting (T) or non-targeting (NT) crRNA, a chimeric *cas* operon targeted by CracrIF1, and either an empty vector (-) or its derivative expressing wild-type

620 (wt) or seed-mutated (mt) CracrIF1 RNAs. The *cas* operon of PA14 was modified by incorporating the
621 *cas* intergenic sequence from NY5506 (containing the target of CracrIF1). Error bars, mean±s.d. (n=3).
622 (**D**) The RNA level of *csy1* relative to *cas3* in PAO1 cells expressing the wild-type or mutated CracrIF1.
623 Error bars, mean±s.d. (n=3).
624

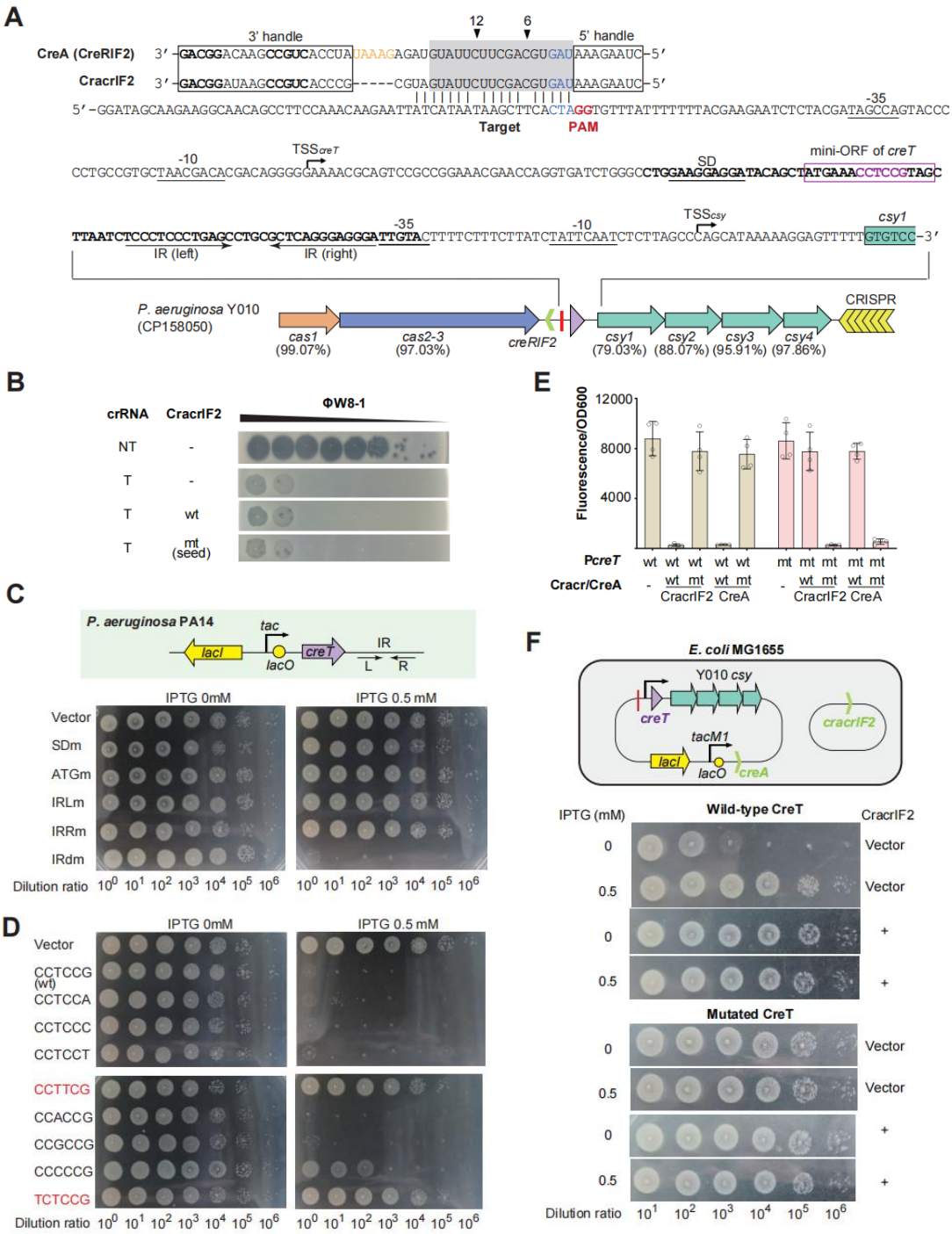

Fig. 3. CracrIF2 transcriptionally inhibits a distinct CreT toxin.
(**A**) Illustration showing the targeting potential of CracrIF2 and CreA (CreRIF2) to the promoter of the CreT toxin (P_{creT}) from *P. aeruginosa* Y010. Nucleotides complementary to PAM are in red. Mismatches at positions 6 and 12 (respective to PAM) are indicated. The identical ΨS nucleotides shared by CracrIF2 and CreA are shaded in gray, with the extra nucleotides in CreA shown in orange. Blue nucleotides were mutated in panels **B** and **E**. Nucleotides of 5' and 3' handles are framed. Palindromic nucleotides within 3' handle are in bold. TSS information was obtained by 5' RACE (see fig. S6). The sequence of *creT* is bolded. IR, inverted repeats. Sequence similarities shared by PA14 and Y010 Cas proteins are noted. (**B**)

636 PFUs of ΦW8-1 infecting PAO1 cells with a phage-targeting (T) or non-targeting (NT) crRNA, a
637 chimeric *cas* operon (PA14-Y010) targeted by CracrIF2, and either an empty vector (-) or its derivative
638 expressing wild-type (wt) or seed-mutated (mt) CracrIF2 RNAs. (**C**) Growth of PA14 cells expressing
639 a series of CreT mutants (controlled by an IPTG-inducible *tac* promoter containing the *lacO* operator).
640 (**D**) Synonymous and non-synonymous (highlighted in red) mutation analyses of the two consecutive
641 proline codons of CreT. The wild-type (wt) sequence is CCTCCG. (**E**) Fluorescence intensity from
642 PAO1 cells containing a P_{creT}-controlled *mCherry* gene. Three seed nucleotides (highlighted in blue in
643 panel **A**) of CracrIF2 and CreA were mutated (mt). wt, wild-type. Error bars, mean±s.d. (n=4). (**F**)
644 Growth of PAO1 cells with a plasmid containing the Y010 *csy* operon, *creT* (controlled by its native
645 promoter), and an IPTG-inducible *creA*, along with a second plasmid expressing CracrIF2 RNAs (or its
646 empty vector control).

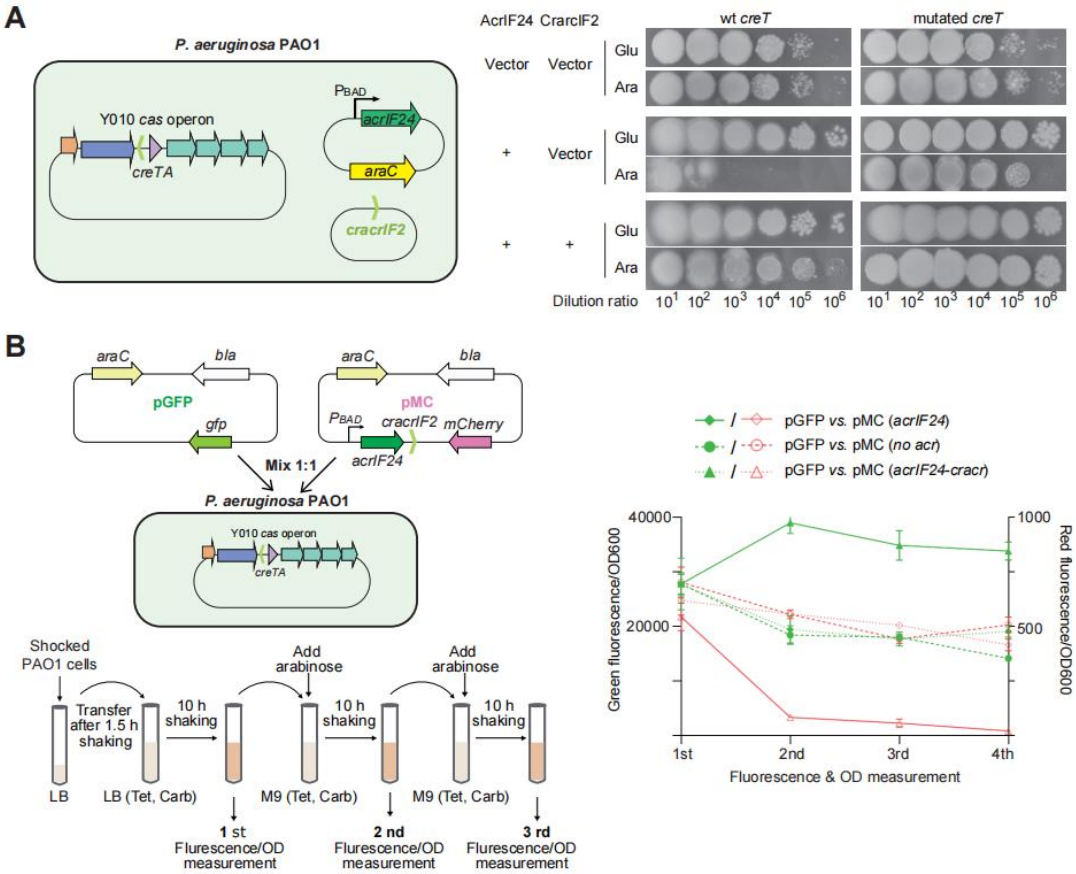

Fig. 4. CracrIF2 blocks abortive infection induced by Y010 CreTA.
(**A**) Schematic representation (left) and results (right) of the assay to evaluate the ability of CracrIF2 RNAs to alleviate the CreTA cytoxicity that is triggered by AcrIF24 expression. AcrIF24 expression is controlled by the arabinose-inducible BAD promoter (P_{BAD}), with glucose used to suppress any basal activity of P_{BAD}. In the mutated *creT* control, the two critical proline codons were removed. (**B**) Schematic representation (left) and results (right) of the assay to assess the anti-CreTA function of CracrIF2. PAO1 cells carrying the Y010 *cas* operon were electrotransformed with two reporter plasmids (pGFP and pMC, mixed in a 1:1 ratio). M9, a minimal medium. Tet, tetracycline; Carb, carbenicillin. Error bars, mean±s.d. (n=3).

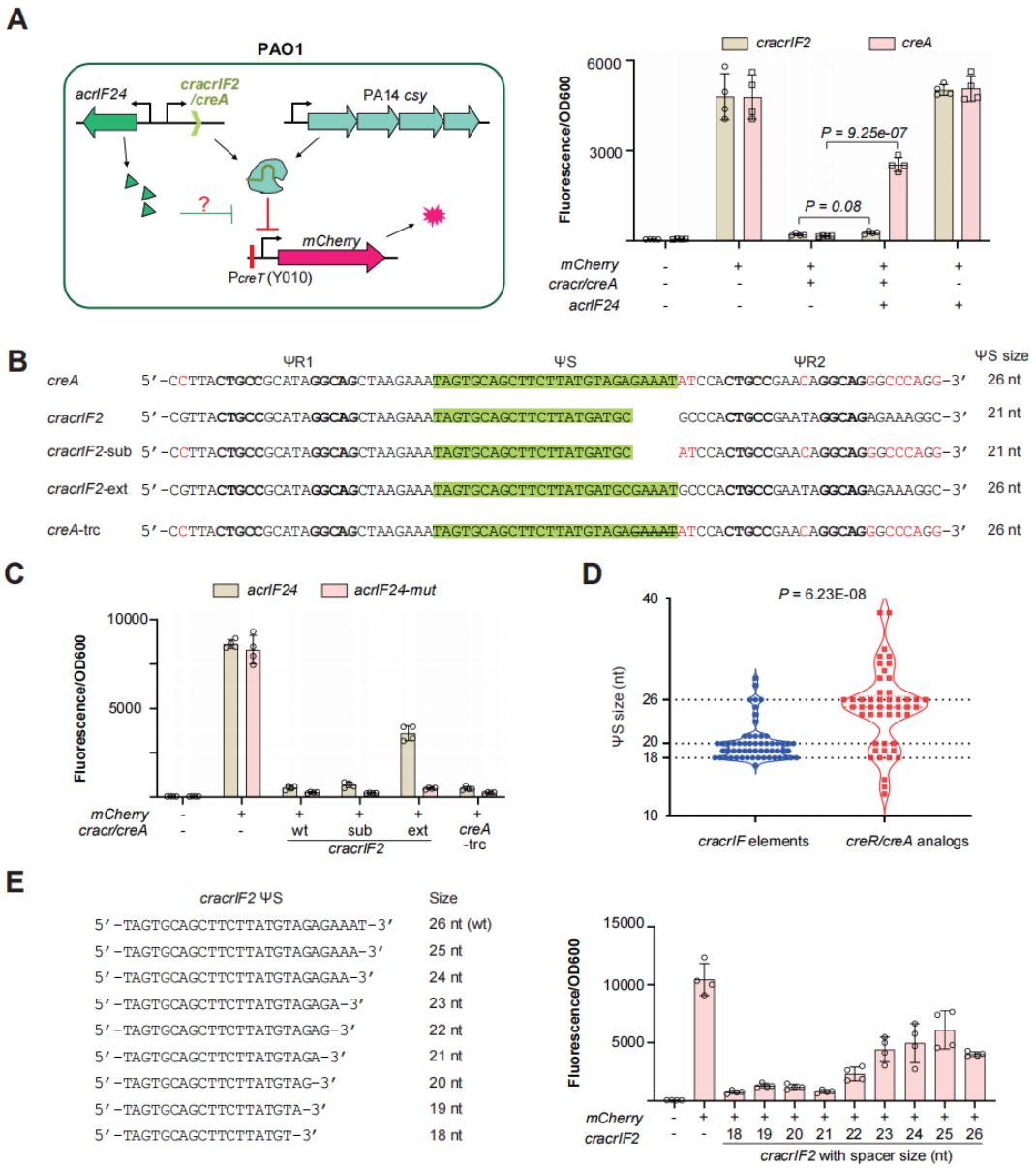

Fig. 5. AcrIF24 differentiates between CracrIF2 and CreA (CreRIF2) based on their differing spacer sizes.

(**A**) Fluorescence intensity of PAO1 cells containing a plasmid expressing mCherry under the control of the Y010 *creT* promoter (targeted by its corresponding CreA and the viral CracrIF2), a second plasmid expressing PA14 Csy proteins, and a third plasmid expressing CracrIF2 or CreA with or without the co-expression of AcrIF24. (**B**) Illustration showing the sequence differences between *creA*, *cracrIF2* and their ΨR-substituted (sub), ΨS-extended (ext), or ΨS-truncated (trc) mutants. (**C**) The inhibitory effects of the mutated CracrIF2 or CreA on their target promoter in the presence of AcrIF24 or its mutant. (**D**) Distribution of the spacer size of all discovered *cracrIF* and related *creR/creA* elements. (**E**) Impact of spacer size on the regulatory activity of CracrIF2 RNAs in the presence of AcrIF24. Error bars, mean± s.d. (n=4). *P* values were calculated from two-sided *t*-test.

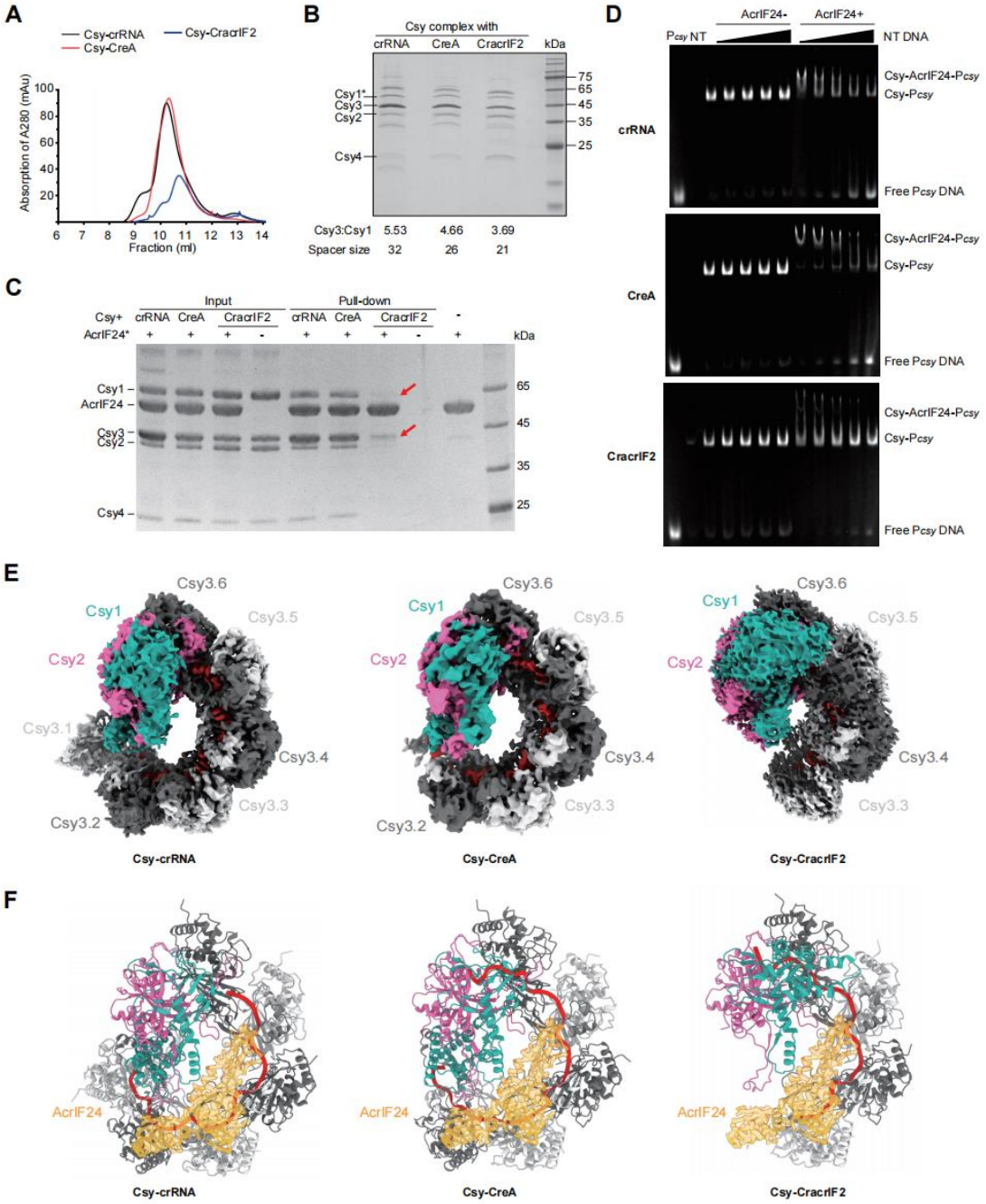

Fig. 6. The interaction of AcrIF24 with Csy complexes assembled with crRNA, CreA, or CracrIF2. (**A**) SEC traces show co-expressed Csy1-4 proteins (with His*6 tagged Csy1) with crRNA, CreA, or CracrIF2 in *E. coli*. mAU, milliabsorbance units. (**B**) SD-PAGE analysis of peak fractions purified by SEC. The molar ratio of Csy3 and Csy1 was estimated based on band intensities and molecular weights. (**C**) GST-labeled AcrIF24 pull-down experiments with Csy proteins bound to crRNA, CreA, or CracrIF2. Red arrows indicate the inefficiently captured Csy1 and Csy3 proteins in the CracrIF2 assay. (**D**) Competition assay with non-target DNA (0, 0.15, 0.3125, 0.625, or 1.25 μM) and FAM-labeled target P_{csy} DNA (0.04 μM) for 0.8 μM Csy-crRNA, Csy-CreA, or Csy-CracrIF2 complexes in the absence or presence of AcrIF24 proteins (9.6 μM). (**E**) Overall structures of the Csy complex assembled with crRNA, CreA, or CracrIF2. The Csy3 subunits are numbered according to the canonical Csy complex with crRNA. (**F**) Structural superimposition between Csy-AcrIF24 and Csy-crRNA, Csy-CreA, or Csy-

684 CracrIF2. Only AcrIF24 monomer is shown for the Csy-AcrIF24 structure.
685

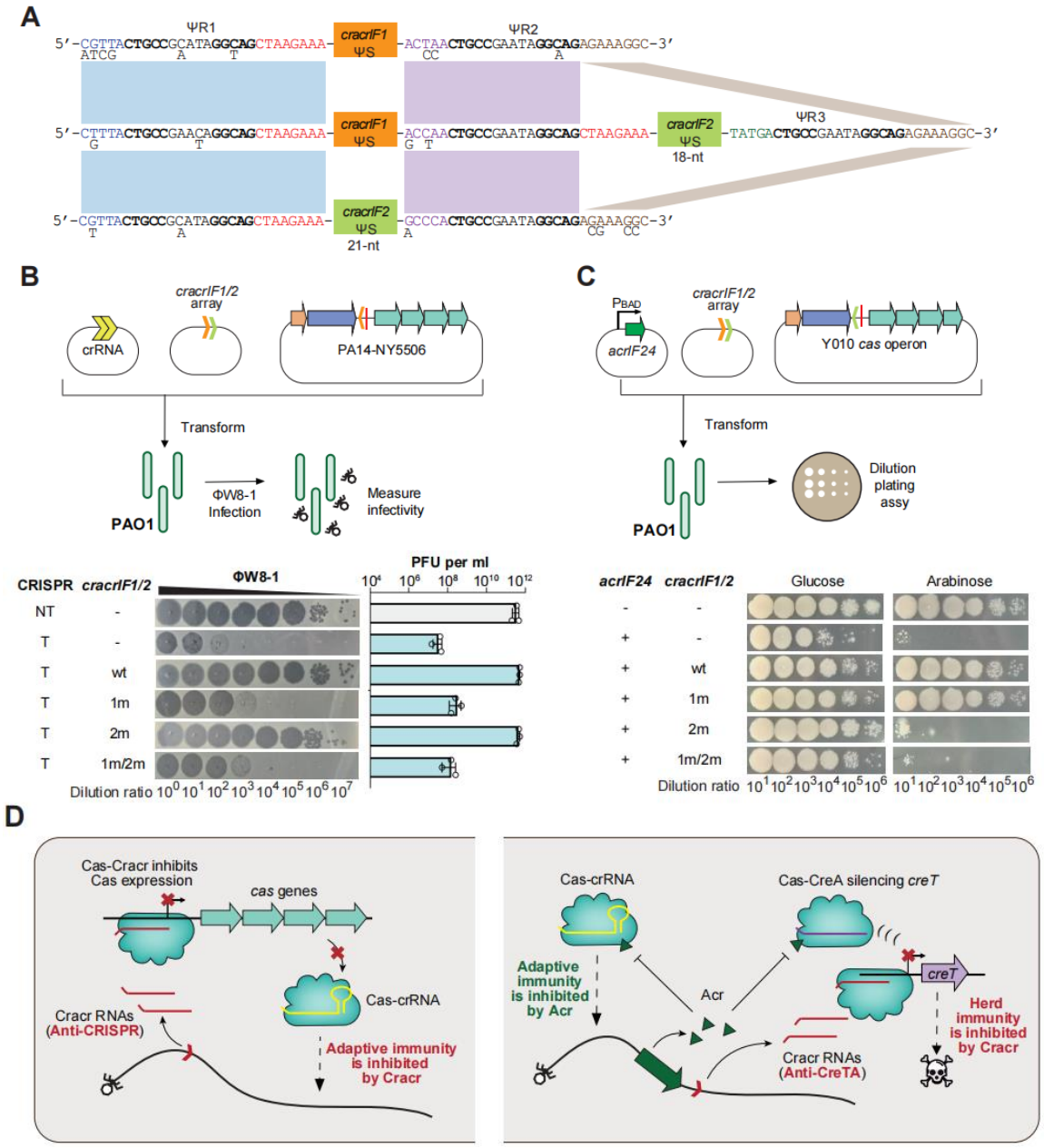

Fig. 7. A Cracr array can inhibit both adaptive and innate defenses.
(**A**) Illustration showing the homology among ΨR sequences from the *cracrIF1/2* array and the standalone *cracrIF* genes. Nucleotide substitutions observed for each ΨR unit are indicated below the sequence. Signature 5'-end nucleotides for each ΨR are highlighted in blue (ΨR1), purple (ΨR2), and green (ΨR3 of the array). Conserved nucleotides producing a 5'-handle on mature Cracr RNAs are highlighted in red. Palindromic nucleotides within each ΨR are shown in bold. (**B**) PFUs of ΦW8-1 infecting PAO1 cells with a phage-targeting (T) or non-targeting (NT) crRNA, a chimeric *cas* operon (PA14-NY5506) targeted by CracrIF1, and either an empty vector (-) or a vector expressing the Cracr array (+). The two ΨS sequences of the Cracr array were individually mutated (1m and 2m) or simultaneously mutated (1m/2m). Error bars, mean±s.d. (n=3). (**C**) Growth of PAO1 cells containing the Y010 *cas* operon, the Cracr array, and an P_{BAD}-controlled *acrIF24* gene. Glucose or arabinose was used to inhibit or induce AcrIF24 expression. (**D**) Model illustrating how Cracr RNAs targeting the promoter of Cas proteins or a CreT toxin undermine the CRISPR adaptive immunity or the toxin-

701 induced innate/herd immunity, respectively.
702

References.

1. R. Barrangou, P. Horvath, A decade of discovery: CRISPR functions and applications. *Nat Microbiol* **2**, 17092 (2017). doi:10.1038/nmicrobiol.2017.92
2. F. Hille, H. Richter, S. P. Wong, M. Bratovic, S. Ressel, E. Charpentier, The Biology of CRISPR-Cas: Backward and Forward. *Cell* **172**, 1239-1259 (2018). doi:10.1016/j.cell.2017.11.032
3. P. M. Nussenzweig, L. A. Marraffini, Molecular Mechanisms of CRISPR-Cas Immunity in Bacteria. *Annu Rev Genet* **54**, 93-120 (2020). doi:10.1146/annurev-genet-022120-112523
4. K. S. Makarova, Y. I. Wolf, J. Iranzo, S. A. Shmakov, O. S. Alkhnbashi, S. J. J. Brouns, E. Charpentier, D. Cheng, D. H. Haft, P. Horvath, S. Moineau, F. J. M. Mojica, D. Scott, S. A. Shah, V. Siksnys, M. P. Terns, C. Venclovas, M. F. White, A. F. Yakunin, W. Yan, F. Zhang, R. A. Garrett, R. Backofen, J. van der Oost, R. Barrangou, E. V. Koonin, Evolutionary classification of CRISPR-Cas systems: a burst of class 2 and derived variants. *Nat Rev Microbiol* **18**, 67-83 (2020). doi:10.1038/s41579-019-0299-x
5. E. Semenova, M. M. Jore, K. A. Datsenko, A. Semenova, E. R. Westra, B. Wanner, J. van der Oost, S. J. J. Brouns, K. Severinov, Interference by clustered regularly interspaced short palindromic repeat (CRISPR) RNA is governed by a seed sequence. *Proc Natl Acad Sci U S A* **108**, 10098-10103 (2011). doi:10.1073/pnas.1104144108
6. B. Wiedenheft, E. van Duijn, J. Bultema, S. Waghmare, K. H. Zhou, A. Barendregt, W. Westphal, A. Heck, E. Boekema, M. Dickman, J. A. Doudna, RNA-guided complex from a bacterial immune system enhances target recognition through seed sequence interactions. *Proc Natl Acad Sci U S A* **108**, 10092-10097 (2011). doi:10.1073/pnas.1102716108
7. H. K. Ratner, A. Escalera-Maurer, A. Le Rhun, S. Jaggavarapu, J. E. Wozniak, E. K. Crispell, E. Charpentier, D. S. Weiss, Catalytically Active Cas9 Mediates Transcriptional Interference to Facilitate Bacterial Virulence. *Mol. Cell* **75**, 498–510 (2019). doi:10.1016/j.molcel.2019.05.029
8. M. Li, L. Gong, F. Cheng, H. Yu, D. Zhao, R. Wang, T. Wang, S. Zhang, J. Zhou, S. A. Shmakov, E. V. Koonin, H. Xiang, Toxin-antitoxin RNA pairs safeguard CRISPR-Cas systems. *Science* **372**, 6541 (2021). doi:10.1126/science.abe5601
9. S. A. Shmakov, Z. K. Barth, K. S. Makarova, Y. Wolf, V. Brover, J. E. Peters, E. Koonin, Widespread CRISPR-derived RNA regulatory elements in CRISPR-Cas systems. *Nucleic Acids Res* **51**, 8150-8168 (2023). doi:10.1093/nar/gkad495
10. C. Liu, R. Wang, J. Li, F. Cheng, X. Shu, H. Zhao, Q. Xue, H. Yu, A. Wu, L. Wang, S. Hu, Y. Zhang, J. Yang, H. Xiang, M. Li, Widespread RNA-based *cas* regulation monitors crRNA abundance and anti-CRISPR proteins. *Cell Host Microbe* **31**, 1481-1493 (2023). doi:10.1016/j.chom.2023.08.005
11. R. Wang, X. Shu, H. W. Zhao, Q. Xue, C. Liu, A. C. Wu, F. Y. Cheng, L. Y. Wang, Y. H. Zhang, J. Feng, N. N. Wu, M. Li, Associate toxin-antitoxin with CRISPR-Cas to kill multidrug-resistant pathogens. *Nat Commun* **14**, 2078 (2023). doi:10.1038/s41467-023-37789-y
12. R. E. Workman, T. Pammi, B. T. K. Nguyen, L. W. Graeff, E. Smith, S. M. Sebald, M. J. Stoltzfus, C. W. Euler, J. W. Modell, A natural single-guide RNA repurposes

Cas9 to autoregulate CRISPR-Cas expression. *Cell* **184**, 675–688 (2021). doi:10.1016/j.cell.2020.12.017

13. R. E. Workman, M. J. Stoltzfus, N. C. Keith, C. W. Euler, J. Bondy-Denomy, J. W. Modell, Anti-CRISPR proteins trigger a burst of CRISPR-Cas9 expression that enhances phage defense. *Cell Rep* **43**, 113849 (2024). doi:10.1016/J.Celrep.2024.113849
14. X. Shu, R. Wang, Z. H. Li, Q. Xue, J. J. Wang, J. F. Liu, F. Y. Cheng, C. Liu, H. W. Zhao, C. Y. Hu, J. Li, S. Y. Ouyang, M. Li, CRISPR-repressed toxin-antitoxin provides herd immunity against anti-CRISPR elements. *Nat Chem Biol*, (2024). Advance online publication. doi:10.1038/s41589-024-01693-3
15. H. E. Ledvina, A. T. Whiteley, Conservation and similarity of bacterial and eukaryotic innate immunity. *Nat Rev Microbiol* **22**, 420-434 (2024). doi:10.1038/s41579-024-01017-1
16. M. M. Gaidt, A. Morrow, M. R. Fairgrieve, J. P. Karr, N. Yosef, R. E. Vance, Self-guarding of MORC3 enables virulence factor-triggered immunity. *Nature* **600**, 138-142 (2021). doi:10.1038/s41586-021-04054-5
17. J. L. Dangl, J. D. G. Jones, Plant pathogens and integrated defence responses to infection. *Nature* **411**, 826-833 (2001). doi:10.1038/35081161
18. S. Camara-Wilpert, D. Mayo-Muñoz, J. Russel, R. D. Fagerlund, J. S. Madsen, P. C. Fineran, S. J. Sorensen, R. Pinilla-Redondo, Bacteriophages suppress CRISPR-Cas immunity using RNA-based anti-CRISPRs. *Nature* **623**, 601–607 (2023). doi:10.1038/s41586-023-06612-5
19. S. Chowdhury, J. Carter, M. F. Rollins, S. M. Golden, R. N. Jackson, C. Hoffmann, L. Nosaka, J. Bondy-Denomy, K. L. Maxwell, A. R. Davidson, E. R. Fischer, G. C. Lander, B. Wiedenheft, Structure Reveals Mechanisms of Viral Suppressors that Intercept a CRISPR RNA-Guided Surveillance Complex. *Cell* **169**, 47–57 (2017). doi:10.1016/j.cell.2017.03.012
20. M. L. Zhang, R. C. Peng, Q. Peng, S. Liu, Z. T. Li, Y. Q. Zhang, H. Song, J. Yang, X. Xing, P. Y. Wang, J. X. Qi, G. F. Gao, Mechanistic insights into DNA binding and cleavage by a compact type I-F CRISPR-Cas system in bacteriophage. *Proc Natl Acad Sci U S A* **120**, e2215098120 (2023). doi:10.1073/pnas.2215098120
21. F. Cheng, R. Wang, H. Yu, C. Liu, J. Yang, H. Xiang, M. Li, Divergent degeneration of *creA* antitoxin genes from minimal CRISPRs and the convergent strategy of tRNA-sequestering CreT toxins. *Nucleic Acids Res* **49**, 10677-10688 (2021). doi:10.1093/nar/gkab821
22. P. Huter, S. Arenz, L. V. Bock, M. Graf, J. O. Frister, A. Heuer, L. Peil, A. L. Starosta, I. Wohlgemuth, F. Peske, J. Novácek, O. Berninghausen, H. Grubmüller, T. Tenson, R. Beckmann, M. V. Rodnina, A. C. Vaiana, D. N. Wilson, Structural Basis for Polyproline-Mediated Ribosome Stalling and Rescue by the Translation Elongation Factor EF-P. *Mol Cell* **68**, 515–527 (2017). doi:10.1016/j.molcel.2017.10.014
23. R. Krafczyk, F. Qi, A. Sieber, J. Mehler, K. Jung, D. Frishman, J. Lassak, Proline codon pair selection determines ribosome pausing strength and translation efficiency in bacteria. *Commun Biol* **4**, 589 (2021). doi:10.1038/s42003-021-02115-z
24. L. G. Yang, L. X. Zhang, P. P. Yin, H. Ding, Y. Xiao, J. W. Zeng, W. H. Wang, H. Zhou, Q. S. Wang, Y. Zhang, Z. L. Chen, M. J. Yang, Y. Feng, Insights into the

inhibition of type I-F CRISPR-Cas system by a multifunctional anti-CRISPR protein AcrIF24. *Nat Commun* **13**, 1931 (2022). doi:10.1038/S41467-022-29581-1

25. A. L. Borges, A. R. Davidson, J. Bondy-Denomy, The Discovery, Mechanisms, and Evolutionary Impact of Anti-CRISPRs. *Annu Rev Virol, Vol* **4**, 37-59 (2017). doi:10.1146/annurev-virology-101416-041616
26. N. Jia, D. J. Patel, Structure-based functional mechanisms and biotechnology applications of anti-CRISPR proteins. *Nat Rev Mol Cell Biol* **22**, 563-579 (2021). doi:10.1038/s41580-021-00371-9
27. A. Agapov, K. S. Baker, P. Bedekar, R. P. Bhatia, T. R. Blower, M. A. Brockhurst, C. Brown, C. E. Chong, J. L. Fothergill, S. Graham, J. P. Hall, A. Maestri, S. Mcquarrie, A. Olina, S. Pagliara, M. Recker, A. Richmond, S. J. Shaw, M. Szczelkun, T. B. Taylor, S. van Houte, S. C. Went, E. R. Westra, M. F. White, R. Wright, Multi-layered genome defences in bacteria. *Curr Opin Microbiol* **78**, 102436 (2024). doi:10.1016/J.Mib.2024.102436
28. J. Lei, J. Frank, Automated acquisition of cryo-electron micrographs for single particle reconstruction on an FEI Tecnai electron microscope. *J Struct Biol* **150**, 69-80 (2005). doi:10.1016/j.jsb.2005.01.002
29. S. Q. Zheng, E. Palovcak, J. P. Armache, K. A. Verba, Y. Cheng, D. A. Agard, MotionCor2: anisotropic correction of beam-induced motion for improved cryo-electron microscopy. *Nat methods* **14**, 331-332 (2017). doi:10.1038/nmeth.4193.
30. A. Punjani, J. L. Rubinstein, D. J. Fleet, M. A. Brubaker, cryoSPARC: algorithms for rapid unsupervised cryo-EM structure determination. *Nat methods* **14**, 290-296 (2017). doi:10.1038/nmeth.4169
31. J. Abramson, J. Adler, J. Dunger, R. Evans, T. Green, A. Pritzel, O. Ronneberger, L. Willmore, A. J. Ballard, J. Bambrick, S. W. Bodenstein, D. A. Evans, C. C. Hung, M. O'Neill, D. Reiman, K. Tunyasuvunakool, Z. Wu, A. Zemgulyte, E. Arvaniti, C. Beattie, O. Bertolli, A. Bridgland, A. Cherepanov, M. Congreve, A. I. Cowen-Rivers, A. Cowie, M. Figurnov, F. B. Fuchs, H. Gladman, R. Jain, Y. A. Khan, C. M. R. Low, K. Perlin, A. Potapenko, P. Savy, S. Singh, A. Stecula, A. Thillaisundaram, C. Tong, S. Yakneen, E. D. Zhong, M. Zielinski, A. Zidek, V. Bapst, P. Kohli, M. Jaderberg, D. Hassabis, J. M. Jumper, Accurate structure prediction of biomolecular interactions with AlphaFold 3. *Nature* **630**, 493-500 (2024). doi:10.1038/s41586-024-07487-w
32. E. F. Pettersen, T. D. Goddard, C. C. Huang, G. S. Couch, D. M. Greenblatt, E. C. Meng, T. E. Ferrin, UCSF Chimera--a visualization system for exploratory research and analysis. *J Comput Chem* **25**, 1605-1612 (2004). doi:10.1002/jcc.20084
33. P. Emsley, K. Cowtan, Coot: model-building tools for molecular graphics. *Acta Crystallogr D Biol Crystallogr* **60**, 2126-2132 (2004). doi:10.1107/S0907444904019158
34. P. V. Afonine, B. K. Poon, R. J. Read, O. V. Sobolev, T. C. Terwilliger, A. Urzhumtsev, P. D. Adams, Real-space refinement in PHENIX for cryo-EM and crystallography. *Acta Crystallogr D Struct Biol* **74**, 531-544 (2018). doi:10.1107/S2059798318006551

Materials and Methods

Bacterial stains and growth conditions

The bacterial strains used in this study are shown in Table S3. *P. aeruginosa* strains (PA14 and PAO1) and *E. coli* strains (DH5α, Mg1655, BL21(DE3)) were cultured at 37°C in lysogeny broth (LB) shaken at 200 rpm or LB-Agar (LBA) plates containing 1.2% (w/v) agar. When applicable, antibiotics were added at the following concentration: ampicillin (Amp), 100 mg L^{-1}; chloramphenicol (Cm), 25 mg L^{-1}; streptomycin (Str), 50 mg L^{-1}; tetracycline (Tet), 50 mg L^{-1}; kanamycin (Kan), 50 mg L^{-1}; carbenicillin (Car), 300 mg L^{-1} for *P. aeruginosa* and 100 mg L^{-1} for *E. coli*; gentamicin (Gen), 50 mg L^{-1} for *P. aeruginosa* and 15 mg L^{-1} for *E. coli*; isopropyl β-D-1-thiogalactopyranoside (IPTG), 500 μM; L-arabinose (Ara), 0.3% (w/v); Glucose (Glu), 0.5% (w/v).

Phage purification and titration

The phage used in this study are listed in Table S3. 1 mL of overnight host culture was inoculated into 100 mL LB and incubated for one hour. Thereafter, a single plaque containing the phage from a top agar was transferred to the culture and incubated overnight. Centrifugation (4000 rpm for 10 min at 4°C) then separates the phage from the cellular debris. The supernatant was further sterilized by filtration using a 0.22 μm filter and stored in a sterile tube. Last, the phage titre was determined by pipetting 5 μL drops of serial dilutions of the phage stock in SM buffer (100 mM $CaCl_2$, 8 mM $MgSO_4$, 50 mM Tris-HCl pH 7.5, 0.01% w/v gelatin) onto an LBA overlay (0.5% w/v) seeded with 200 μL host overnight culture, plaques were counted after incubation overnight. The *P. aeruginosa* phage (ΦW8-1, PQ030834) was amplified on PAO1, and the phages were stored in SM buffer over chloroform.

DNA isolation and manipulation

The oligonucleotides used in this study are listed in Table S3. The DNA polymerases, restriction enzymes, Gibson Assembly mix and T4 DNA ligase were obtained from Vazyme or New England Biolabs. DNA form agarose gels or PCR was purified using the E.Z.N.A.® Gel Extraction Kit (OMEGA). PCR, Restriction digest, Gibson Assembly, ligations and *E. coli* transformations following the standard guidelines. Plasmid DNA was extracted from overnight cultures using the EasyPure Plasmid Miniprep Kit (Transgen), and confirmed by Sanger sequencing is necessary.

Plasmids and their construction details are listed in Table S3. The pRSF1010 and pVS1 related plasmids were introduced into *P. aeruginosa* strains by conjugation with *E. coli* S17 strains. In brief, the overnight cultures of PAO1 and *E. coli* S17-λpir containing the plasmid were mixed in a 1:2 (recipient: donor) ratio for conjugation. The mixed cells were centrifuged at 7000 rpm for 2 min to pellet the cells, then 100 μl of LB resuspended the pellet. The mixed cultures were spotted onto a 0.45 μM sterile filter membrane in the LBA plates and incubated at 37°C for 10 h. Conjugation spots were collected and resuspended in LB, then conjugation cultures were plated on Pseudomonas Isolation Agar (BD Difco) plates supplemented with responsive antibiotics. Other plasmids were introduced into *P. aeruginosa* or *E. coli* strains by electroporation using standard techniques.

Bioinformatics search for Cracrs in databases

Known CreR sequences of types IF and IE were utilized as queries for BLASTn

880 (v2.5.0+) searches against the NCBI RefSeq, IMG/VR, and IMG/PR databases. The
881 BLASTn search was performed with the following parameters: -reward 1, -penalty -2, -
882 gapopen 4, -gapextend 2, -word_size 6, -dust no, and -evalue 10. CRISPR-Cas-Typer was
883 used to identify and eliminate CRISPR-Cas systems in the genomes corresponding to these
884 BLASTn hits. Finally, the palindromic structures containing typical CRISPR repeat
885 sequences were identified as Cracr by manual screening.
886 Due to the observed co-location pattern between AcrIF24 and Cracr IF, a further
887 search for potential Cracr IF sequences was conducted. Initially, the AcrIF24 profile HMM
888 was used to identify AcrIF24 homologs in the three databases (NCBI RefSeq, IMG/VR,
889 IMG/PR). From these results, 1.5kb upstream and downstream intergenic regions were
890 extracted, ensuring that regions were at least 40bp in length. A BLASTn search was then
891 carried out within these intergenic regions using known CracrIF/CreR sequences as queries,
892 with the following parameters: -reward 1, -penalty -2, -gapopen 5, -gapextend 2, -
893 word_size 7, -dust no, and -evalue 10.

894 Construction of Phylogenetic Tree

895 The AcrIF24 profile HMM was used to search the NCBI RefSeq, IMG/VR, and
896 IMG/PR databases, retaining results with at least 90% sequence coverage. To construct an
897 evolutionary tree for AcrIF24 and *cracr* genes, the retrieved sequences were first aligned
898 using MAFFT (v7.525) with the FFT-NS-1000 algorithm. A phylogenetic tree was then
899 constructed from the aligned sequences using FastTree (v2.1.11), employing gamma-
900 distributed site rates and the WAG evolutionary model. Taxonomic orders are represented
901 by colored rectangles outside the tree. Mobile genetic element (MGE) origins are indicated
902 by symbols at the branch tips, with circles for phages and squares for plasmids.

903 Expression of CracrIF and related constructs

904 For the experiments presented in Fig. 2C, 2D, 3B, 3F and fig. S2B, S5, B and D,
905 CracrIF1 (MN096267: 40,013-40,171bp), CracrIF2 (NZ_JAIWRW010000005: 191,361-
906 191,521bp), CracrIF1/2-array (NZ_JAOXGH010000015: 4,931-5,124) and their variants
907 were expressed from the *Escherichia-Pseudomonas* (ColE1-pRO1600) shuttle vector
908 pRGPDuo4 either under the control of its wild-type promoter. For the fluorescence
909 measurement in Fig. 2B, 3C, 5A, 5C and 5E, CracrIF1 (MN096267: 40,013-40,129bp),
910 CreR1 (CP096927.1: 2,821,988-2,822,107bp), CracrIF2 (NZ_JAIWRW010000005:
911 191,361-191,476bp), CreA2 (CP158050: 2,825,629-2,825751bp) and their variants were
912 expressed with the predicted TSS downstream of the P_{TAC} promoter. CracrIF mutations
913 were cloned by PCR using mismatched primers and overlap PCR. Detailed information on
914 the CracrIF sequences is provided in Table S1, and the primer sequence information is
915 provided in Table S3.

916 Plaque assay

917 Triplicate cultures of hosts carrying either a phage targeting spacer or non-targeting
918 control, and containing a plasmid expressing a candidate Cracr, Cracrmut or empty vector
919 control were grown overnight. Then, 150 μL of the culture was mixed into 3 mL of molted
920 top agar (0.7%, w/v) supplemented with 10 mM $MgSO_4$ and corresponding antibiotics, and
921 the mixture was poured over an LBA plate containing with 10 mM $MgSO_4$ and antibiotics
922 as needed. After allowing the top agar to solidify at room temperature, 2.5 μL drops of 10-
923 fold serial dilutions of the phage reservoir were spotted on the surface. The plates were

924 incubated upright at 37°C overnight. Plaques were counted and expressed as the plaque
925 forming units (PFU) mL^{-1}.

926 Fluorescence measurement

927 To evaluate the activity of *csy* or *creT* promoter, PCR amplified the promoter
928 sequence (containing the promoter and targeted sequence) and its variants, the *mCherry*
929 gene, respectively, and then were cloned on the pVS1 plasmid. The plasmid was then
930 introduced into the PAO6 strains (PAO1 strain carries the *csy1-4* operon expressed with
931 P_{J23116}.) along with another plasmid expressing Cracr or CreA.

932 For the experiments presented in Fig. 5, A, C and E and fig. S8, we constructed the
933 constitutive promoter J23119 to express the AcrIF24 protein in the reverse transcriptional
934 orientation to that of CracrIF or CreR/CreA, thus avoiding any potential interference. The
935 constructed plasmids were introduced into PAO6 strains for subsequent fluorescence
936 measurements.

937 To evaluate the activity of *casA* promoter, PCR amplified the promoter sequence
938 (containing the promoter and targeted sequence) and its variants, the *gfp* gene, respectively,
939 and then were cloned on the pET28a plasmid. The plasmid was then introduced into the *E.*
940 *coli* MG1655::P_{tacm2}-CasA-E (MG1655::Cas) strains along with another pACYC plasmid
941 expressing CracrIE or CreRIE.

942 Three or more biological replicates were included in each experimental set. The
943 transformants were inoculated into 3 mL of LB supplemented with corresponding
944 antibiotics, and incubated overnight. 200 μL of the cultures for measurement of
945 fluorescence intensity and optical density at 600 nm (OD600) using the Synergy H4 Hybrid
946 multimode microplate reader (BioTeck). For each biological replicate, the ratio of
947 fluorescence to OD600 was determined, and the mean and standard deviation were
948 subsequently computed. To conduct the statistical analysis, a two-tailed Student's t-test was
949 applied to ascertain the P values.

950 RNA isolation

951 Overnight cultures were diluted 1:100 into 10 mL LB supplemented corresponding
952 antibiotics, and grown at 37°C until logarithmic phase. Centrifuge 2 mL of culture at 7000
953 rpm for 2 min at 4°C to pellet the cells, then the total RNA was extracted from the pellet
954 using E.Z.N.A. Bacterial RNA kit (Omega), following the standard guidelines. Residual
955 genomic DNA was removed using DNase I (New England Biolabs) according on the
956 manufacture's instruction. RNA concentration were determined using a NanoDrop One
957 Spectrophotometer (Thermo Fisher Scientific).

958 5' RACE

959 To identify the transcription start-site (TSS) of the *csy1*, 5' RACE was used to
960 identify the TSS of the mRNA transcript using the template-switching enzyme (New
961 England Biolabs). In brief, 1μg of the total RNA was mixed with 1mM *csy1*-specific
962 reverse primer, the mixture was incubated at 85°C for 5 min and then immediately placed
963 on ice. Afterwards, a template-switching reverse-transcription reaction was used to
964 generate cDNAs with a universal sequence of choice (introduced by a template-switching
965 oligonucleotide) attached to the 3' end of the cDNA (New England Biolabs). The
966 transcripts of mRNA were identified by PCR amplification with primers that bind upstream
967 from the *csy1*-RT-primers site and in the template-switching oligonucleotide, respectively.

968 PCR products were verified on a gel and verified by Sanger sequencing (PAO1_Y010,
969 PAO1 strain carries the CRISPR-Cas system from PA_Y010) or cloned into the pET28a
970 vector (PAO1_NY5506, PAO1 strain carries the CRISPR-Cas system from PA_NY5506),
971 then plasmids were isolated from individual colonies and subjected to Sanger sequencing.

972 Primer extension analysis

973 The 5′-FAM-labeled mCherry-specific primer as the reverse transcription primer.
974 30 μg of the total RNA was mixed with 2.5 μg of the labeled primer, and reverse
975 transcription was performed using 200 U of the M-MLV reverse transcriptase (Promega,),
976 following the standard guidelines. The extension products were screened using the ABI
977 3730xl DNA Analyzer (Thermo Fisher Scientific), and the results were visualized using
978 Peak Scanner Software v1.0.

979 Small RNA sequencing and analysis

980 A total of 50 μg of RNA was treated with T4 polynucleotide kinase (New England
981 Biolabs) according to the manufacture's protocol. The RNA was purified using the phenol-
982 chloroform method and then precipitated with an equal volume of isopropanol and 0.1
983 volume of 3M sodium acetate. The RNA molecules ranging from 30 to 300 nt were selected
984 to construct a small RNA library with the NEXTFLEX Small RNA-Seq Kit (Bioo
985 Scientific) and then subjected to Illumina HiSeq sequencing (paired-end, 150-bp reads).
986 The raw data was processed to remove adapters. The resulting reads were mapped to the
987 *CracrIF2* or *creA2* sequence using custom Perl scripts.

988 Northern bolt analysis

989 To detect transcription and processing products of CracrIF, biotin-labeled probes
990 were used for northern bolt analysis. In brief, RNA extracted from overnight cultures in
991 triplicate. RNA was mixed with an equal volume of RNA Gel Loading Dye (Thermo Fisher
992 Scientific), heated to 85 ℃ for 5 min and then cooled on ice for 2 min. Then, 10 μg total
993 RNA from each sample was resolved by denaturing 10% TBE-Urea PAGE and was
994 electrotransferred on a Biodyne B nylon membranes (Pall). Membranes were UV-
995 crosslinked, then pre-hybridized 1 hour at 42 ℃, followed by the addition of biotin-labelled
996 ssDNA probe and incubate overnight at 42 ℃. The signal was detected using the
997 Chemiluminescent Nucleic Acid Detection Module Kit (Thermo Fisher Scientific),
998 according to the manufacturer's protocol. The membrane was imaged using the Tanon 5200
999 Multi chemiluminescent imaging system (Tanon Science & Technology). Each blotting
1000 assay was performed with two biological replicates, and a representative result was
1001 provided.

1002 RT-qPCR

1003 The total RNA was treated with DNase I (New England Biolabs) according to the
1004 manufacturer's instructions. cDNA was synthesized using M-MLV Reverse Transciptase
1005 (Promega) and quantified using the SYBR FAST qPCR kit (Kapa Biosystems) on an
1006 Applied Biosystems ViiA^{TM} 7 Real-Time PCR System. The triplicates were analyzed for
1007 each assay based on three independent samples. The primers listed in Table S3.

1008 Dilution plating assay

1009 For the experiments presented in Fig. 3D, 3E and fig. S7. the *creT* and its variants

1010 were cloned into IPTG-inducible vectors, transformed into *P. aeruginosa* PA14 cells and
1011 selected on LB agar plates containing appropriate antibiotic. An individual colony was
1012 inoculated in LB broth containing the appropriate antibiotic, and cultures were allowed to
1013 grow overnight on an incubator shaker to stationary phase. For the experiments presented
1014 in Fig. 3F, the Y010 *creT-csy* operon (CP158050: 2,821,349-2,825,633) and an IPTG-
1015 inducible *creA* gene were cloned into a plasmid with a broad-host-range replication of the
1016 RSF1010 origin of replication. Subsequently, the plasmid was transformed into *E. coli*
1017 MG1655 cells along with another plasmid carrying either the CracrIF2 gene or an empty-
1018 vector control, and selected on LB agar plates containing IPTG and appropriate antibiotic.
1019 An individual colony was inoculated in LB broth containing IPTG and appropriate
1020 antibiotic, and cultures were allowed to grow overnight on an incubator shaker to stationary
1021 phase. 10-fold serial dilutions of these cultures were prepared in LB broth, and 2.0 μL of
1022 these dilutions were spotted on LB agar plates containing the appropriate antibiotic and
1023 with or without 0.5 mM IPTG.

1024 CracrIF2 re-suppresses AcrIF24-destroying CreTA module

1025 To demonstrate the anti-anti-anti-CRISPR function of *cracrIF2* and *cracrIF1/2*
1026 array, carrying CracrIF2 or CracrIF1/2 array and their variants were transformed into the
1027 PAO1_Y010 cells containing L-arabinose-induced expression of AcrIF24, and selected on
1028 LB agar plates containing glucose and appropriate antibiotic. An individual colony was
1029 inoculated in LB broth containing glucose and appropriate antibiotic, and cultures were
1030 allowed to grow overnight on an incubator shaker to stationary phase. 10 fold serial
1031 dilutions of these cultures were prepared in LB broth, and 2.0 μL of these dilutions were
1032 spotted on LB agar plates containing the appropriate antibiotic and with glucose or L-
1033 arabinose.

1034 Stability of the AcrIF24-CracrIF2 plasmid in CreTA- containing strains

1035 For the experiments presented in Fig. 4B, the GFP reporter plasmid (pGFP) and
1036 another mCherry reporter plasmid (pMC) carrying either the L-arabinose-induced *acrIF24*
1037 or the *acrIF24-cracrIF2* were mixed in equal proportions (500ng: 500ng) and transferred
1038 into the PAO1_Y010 strains. After incubation in LB medium for 1.5 h, the culture was
1039 inoculated into fresh LB medium appropriate antibiotic, and fluorescence was measured
1040 after 10 h of incubation. Subsequently, the culture was sub-inoculated (1:100 dilution) in
1041 M9 rich medium (M9 medium supplemented with 10% LB medium) appropriate antibiotic
1042 and L-arabinose. This process was repeated three more times and fluorescence
1043 measurements were taken each time. Each set of tests contained three biological replicates.

1044 Protein expression and purification

1045 Plasmids encoding Csy1-Csy4 and crRNA/Cracr/CreA were co-transformed into *E.*
1046 *coli* strain BL21(DE3). The proteins were expressed in *E. coli* strain BL21 (DE3) and
1047 induced by 0.2 mM IPTG when the cell density reached an OD_{600nm} of 0.8. After growth at
1048 18℃ for 12 h, the cells were harvested, resuspended in lysis buffer (50 mM Tris-HCl pH
1049 8.0, 300 mM NaCl, 10 mM imidazole and 1 mM PMSF) and lysed by sonication. The cell
1050 lysate was centrifuged at 20,000 g for 50 min at 4℃ to remove cell debris. The cleared
1051 lysate was affinity purified using a 5 mL HisTrap™ FF (Cytiva) column equilibrated in
1052 wash buffer containing 50 mM Tris-HCl pH 8.0, 300 mM NaCl, 30 mM imidazole, and
1053 eluted using a gradient against elution buffer (lysis buffer containing 500 mM imidazole).

Elution fractions were concentrated and further purified using a Superdex-200 Increase 10/300 GL (GE Healthcare) column equilibrated with a buffer containing 10 mM Tris-HCl pH 8.0, 200 mM NaCl, 5 mM dithiothreitol. The purified protein was analyzed by SDS-PAGE. To purify AcrIF24, the ORF from *P. aeruginosa* isolate B51 (DAFOPW010000042: 27,513-28,199) was constructed into pGEX-6P-1 plasmid for fusion expression with GST-tag, and subsequently transferred into *E. coli* strain BL21(DE3). GST-AcrIF24 was induced by 0.1 mM IPTG when the cell density reached an OD600nm of 0.8 and then growth at 18°C for 12 h. The purification procedure is the same as cascade except that the GSTrap™ HP (Cytiva) column, lysis buffer (20 mM Hepes pH 7.5, 500 mM NaCl, 1 mM PMSF) and elution buffer (20 mM Hepes pH 7.5, 500 mM NaCl, 10 mM reduced glutathione, 1mM dithiothreitol). The fusion protein was then digested with PreScission protease at 4°C overnight to remove GST-tag.

Cryo-EM sample preparation and data acquisition

4 μL aliquots of cascade complexed with crRNA/CracrIF2/CreA2 protein at a concentration of 4/4.5/1.5 mg/mL were respectively applied to discharged 300-mesh Quantifoil R1.2/1.3 grids (Quantifoil, Micro Tools GmbH, Germany). Grids were blotted for 4.5 s and plunged into liquid ethane using an FEI Mark IV Vitrobot operated at 8°C and 100% humidity.

Cryo-EM data were collected on a 300 kV Titan Krios G3 equipped with a Gatan K3 detector and a GIF Quantum energy filter (slit width of 20 eV). The defocus values ranged from -1.3 μm to -1.8 μm. Each stack of 32 frames was exposed for 2.56 s, and the exposure time of each frame was 0.08 s. The micrographs were automatically collected with the AutoEMation program (*28*) in super-resolution counting mode with a binned pixel size of 0.8374 Å. The total dose of each stack was about 50 e^{-} $Å^{-2}$. The alignment and summation of all 32 frames in each stack were performed using the whole-image motion correction program MotionCor2 (*29*).

Cryo-EM data processing

All cryo-EM data were processed using cryoSPARC (*30*). Contrast transfer function (CTF) parameters were estimated using patch-CTF. Blob picker was used for initial templates generation via 2D classification. Template picker was then used for all particle-picking tasks. For the cascade-crRNA, 732,730 particles were extracted from 928 micrographs. Subsequent two-dimensional (2D) classification, multi-class ab-initio reconstruction, nonuniform refinement and local refinement of the best class were performed, resulting in the resolution of 3.11 Å. Following the same workflow, 2,226,978 particles were extracted from 2,954 micrographs and 1,246,776 particles were extracted from 2,388 micrographs. Subsequently, 146,897 particles were used to resolve the structure of cascade-Cracr at 2.90 Å resolution, and 122,663 particles were used to resolve the structure of cascade-CreA at 3.32 Å resolution, respectively. All structures were determined with C1 symmetry. Resolution is reported using the gold-standard Fourier shell correlation with 0.143 cutoff. See Table S4 for data collection, refinement and validation statistics.

Cryo-EM model building and refinement

The initial models were derived using AlphaFold3 (*31*). We assigned predicted models into our density maps by UCSF ChimeraX (*32*). The models were further optimized by Coot (*33*). The final models of all datasets were refined against the corresponding maps

using PHENIX (*34*) in real space with secondary structure and geometry restraints. The structures were validated through examination of the Clash scores, Molprobity scores and statistics of the Ramachandran plots by PHENIX (Table S4). All the figures were created in PyMOL (*34*) and UCSF ChimeraX.

Electrophoretic mobility shift assay (EMSA)

For EMSA experiments, the His6-tag was tagged to the Csy1 protein, protein purification was performed as described above. To generate dsDNA, the FAM-labelled strand was heated to 98°C in the presence of a twofold excess of an unlabeled complementary strand and allowed to slowly return to room temperature. Specifically, non-target dsDNA without FAM labelling was generated by the same method described above, except that both strands were unlabeled. All full-length single-stranded DNA molecules were synthesized by Tsingke (Beijing, China)**.** Cascade-DNA binding reactions were performed in binding buffer (20 mM HEPES, pH 7.5, 1 mM $MgCl_2$, 150 mM NaCl and 5% glycerol) at 37°C for 15 min. The concentrations of Cascade, dsDNA and AcrIF24 are indicated in the Fig. legends. After the appropriate incubation, the reactions were resolved on native PAGE (6%). The free dsDNA and shifted protein-DNA complexes was detected on a Tanon-5200 Multi instrument (Tanon Science & Technology Co. Ltd.).

CreA-3'FAM:

GCCTTCCAAACAAGAATCACCATAAAAAGCTTCACTAGGCGTTTATTTTT

non-target:

GGCGTTTATGATTTAGTAGGTAATTGGAATTCTGTTGCTTCTATTACTCC

GST pull-down assay

The GST-AcrIF24 fusion protein was mixed with Cascade-crRNA, Cascade-CreA2 and Cascade-CracrIF2, respectively, according to the molecular weight of 1:2 with Mag-MK GST Fusion Protein Purification beads (BBI: C650031). At the same time, only cascade with magnetic beads were used as a negative control. The mixture was gently incubated at 4°C for 3h and then the supernatant was discarded. Then 1 ml pre-cooled wash buffer (20 mM Hepes pH 7.5, 150 mM NaCl, 1% Triton X-100) was added along the wall to wash the magnetic beads, and the washing was repeated for 4 times. Finally, elution buffer (20 mM Hepes pH 7.5, 500 mM NaCl, 10 mM reduced glutathione, 1mM dithiothreitol) was used to eluate the products, the products were tested using SDS-PAGE.

Quantification and statistical analyses

The number of replicates is specified in the associated figure legends. Each replicate represents a biological replicate of the specified experiment. Two-tailed *t*-test was performed for statistical analyses. P-values above 0.05 were considered non-significant. Statistical comparisons for the transformation assays relied on log values, which assumes the samples are normally distributed on a log scale.

1137 **Fig. S1.**

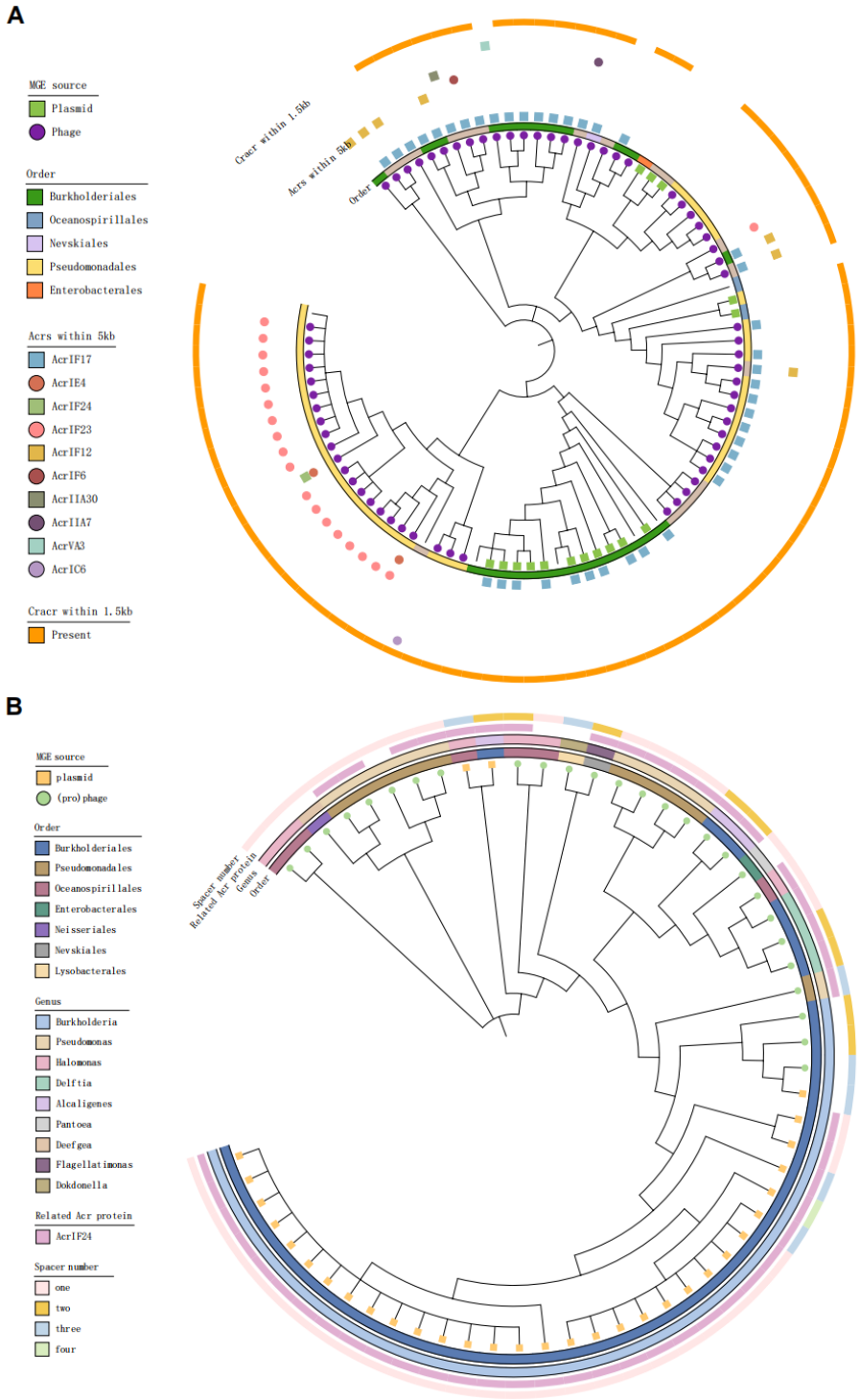

1138

1139

1140 **Fig. S1. Genetic association of *acrIF24* to *cracr* genes.**

1141 (**A**) All *acrIF24* genes from the NCBI RefSeq, IMG/VR and IMG/PR databases were
1142 retrieved and utilized to construct a phylogenetic tree following the removal of redundancy.
1143 Associating *cracr* genes were identified by searching the upstream and downstream 1.5 kb
1144 sequences for each *acrIF24* gene. Other *acr* genes located within a 5 kb distance from each

1145 *acrIF24* gene were also examined. (**B**) Distribution of non-*P. aeruginosa cracr* genes
1146 across different bacterial taxa. Note that *cracr* genes carried by phages (see Table S2) were
1147 not included in this analysis.
1148

Fig. S2.

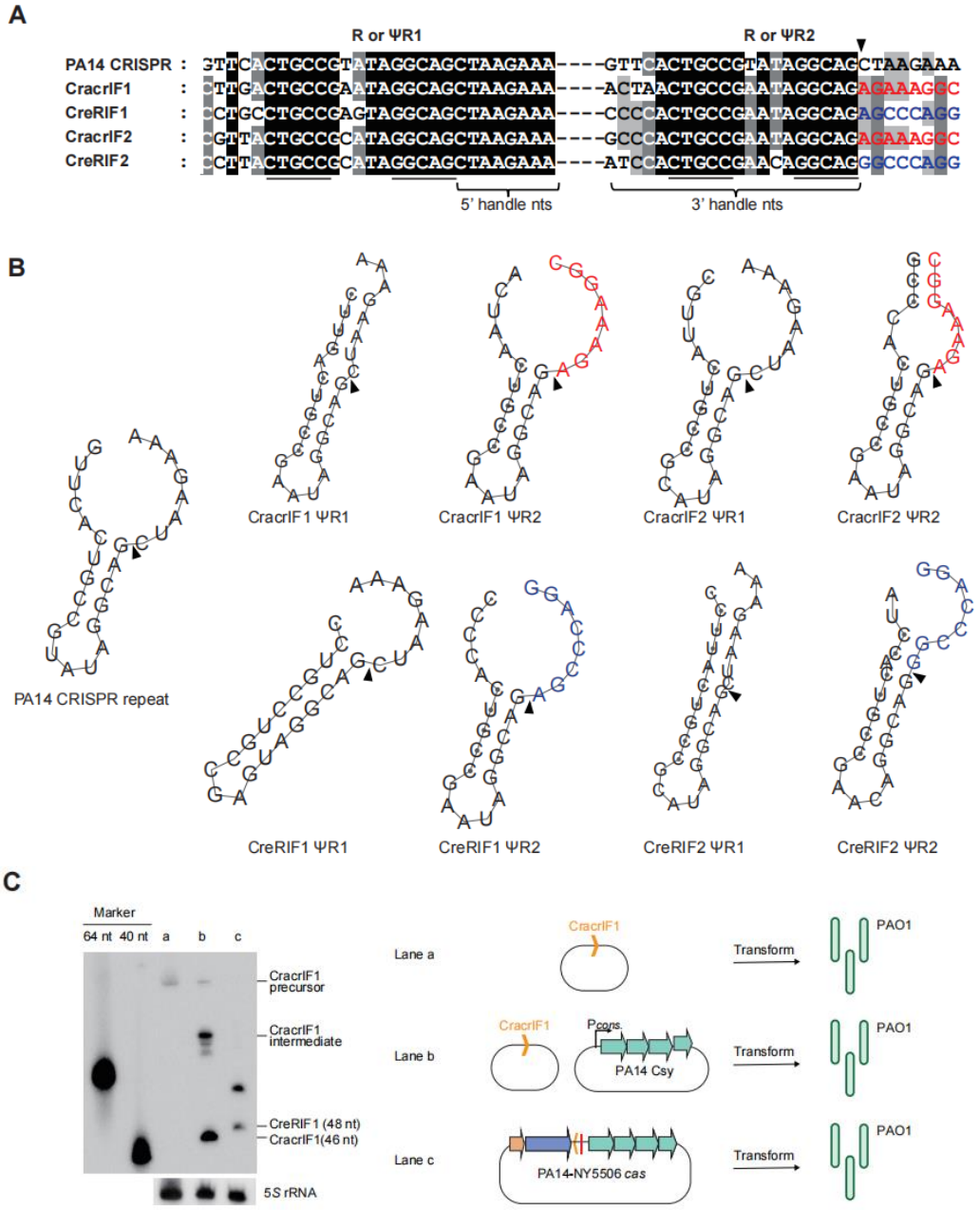

Fig. S2. Sequence and structure conservation among the repeats from *cracr*, *creR*, and CRISPR, and the maturation of CracrIF1 and CreRIF1.
(**A**) Alignment of the ΨR sequences (ΨR1 and ΨR2) from *cracrIF1*, *cracrIF2*, *creRIF1*, *creRIF2* to the typical repeat sequence (R) from the PA14 CRISPR array. Nucleotides (nts) producing a 5' or 3' handle on mature RNAs are indicated. Palindromic nucleotides are underlined. (**B**) Predicted RNA structures of each repeat. Triangles indicate the processing sites by Csy4. ΨR2 nucleotides that evidently differ between *cracrIF* and *creRIF* genes are highlighted in red and blue, respectively. **(C)** Northern blotting analysis of CracrIF1 and CreRIF1 RNAs (using the same probe due to their high sequence similarity). Experimental design is shown on the right. 5*S* rRNA served as the internal control. Biotin-labeled single-

1162 stranded oligos (40 nt or 64 nt) served as markers.

Fig. S3.

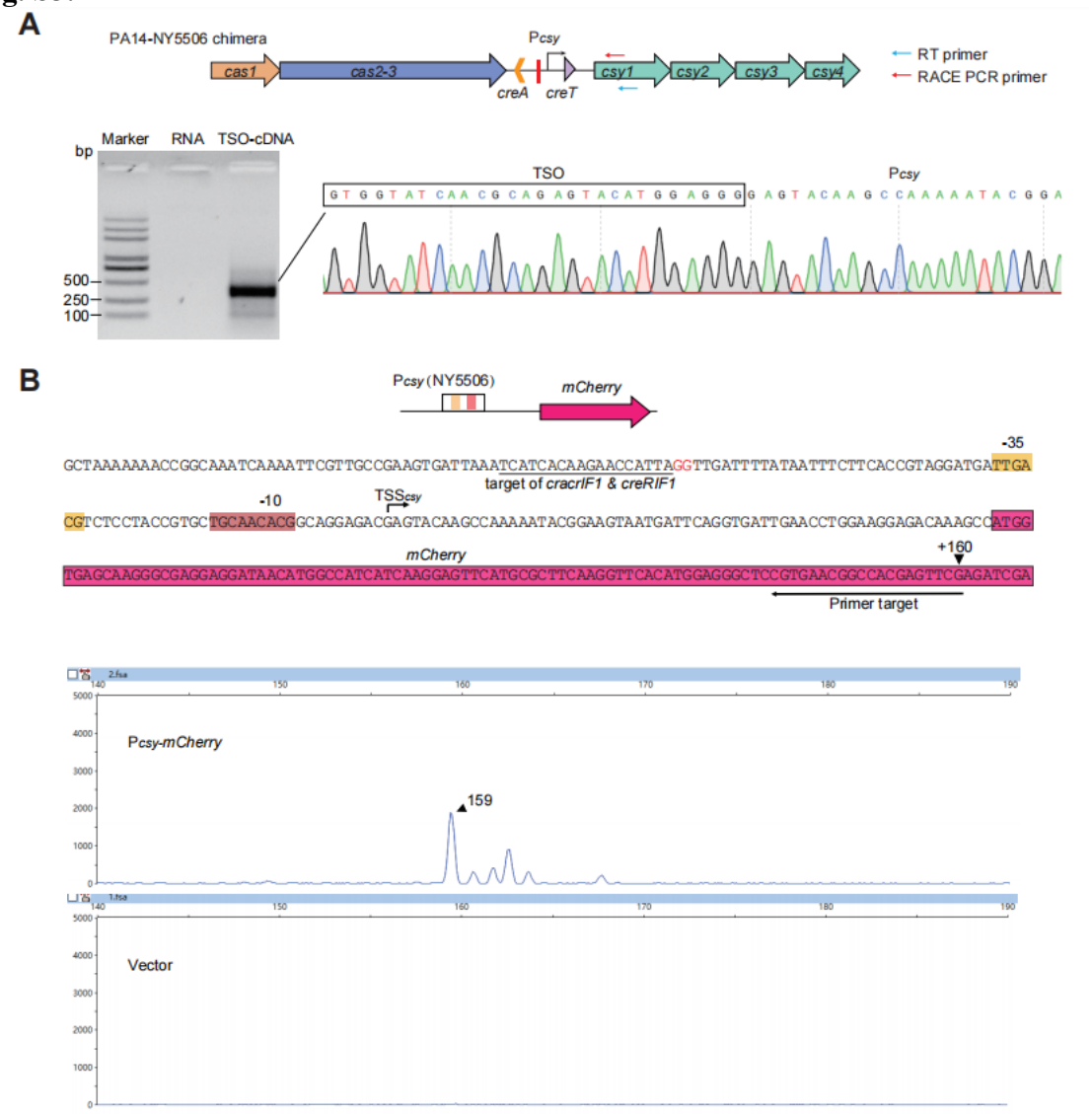

Fig. S3. Characterization of the NY5506 *csy* promoter (P_{csy}).
(**A**) The transcription start site (TSS) of NY5506 *csy* transcripts were determined by 5' RACE. Note that, for convenience, the chimeric *cas* operon PA14-NY5506 used for phage infection experiments was also used for this assay. Complementray DNA (cDNA) was generated by reverse transcription (using RT primer), and subsequently used as the template for PCR reactions with a forward primer against the template switching oligo (TSO) and a reverse primer against *csy1* sequence (RACE PCR primer). DNase-treated RNA samples were used as the negative control. **(B)** Primer extension assay to confirm the TSS of NY5506 P_{csy}. The P_{csy} DNA was first linked to an *mCherry* gene and then introduced into *P. aeruginosa* PAO1 cells, of which total RNA was extracted for primer extension. The primer was designed against the *mCherry* RNA transcript and 5'-labeled by FAM (see the Methods part). The cDNA products of primer extension assay were then subjected to fragment size analysis. PAO1 cells containing an empty vector served as a negative control. Promoter elements -10 and -35 are indicated. The target sequence of CracrIF1 or CreRIF1 RNAs are underlined, with the complementary nucleotides of PAM shown in red.

1180 **Fig. S4.**

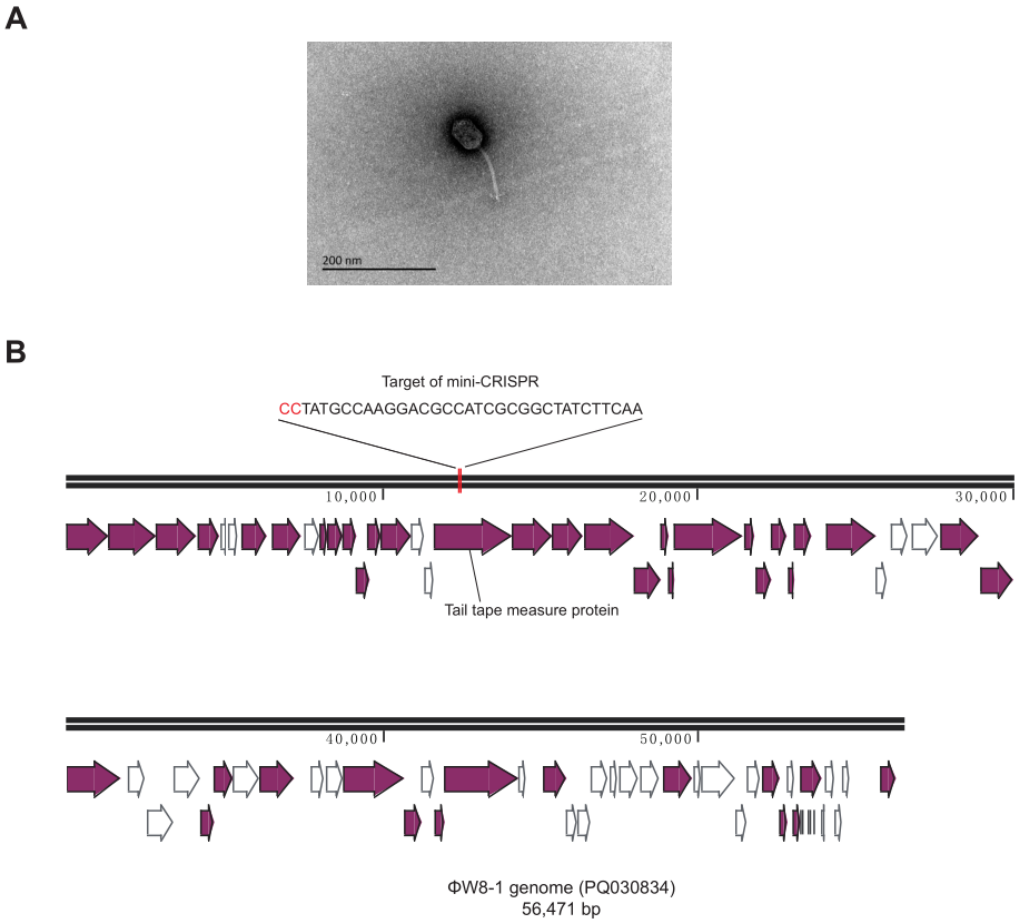

1181
1182 **Fig. S4. Characterization of the ΦW8-1 phage infecting PAO1 cells.**
1183 (**A**) Electron-microscopy of the ΦW8-1 phage. The 200 nm scale bar is given. (**B**) The
1184 genome of ΦW8-1 (with the GenBank ID PQ030834) and design of the mini-CRISPR
1185 targeting the gene of tail tape measure protein. The PAM nucleotides are shown in red.
1186
1187

1188 **Fig. S5.**

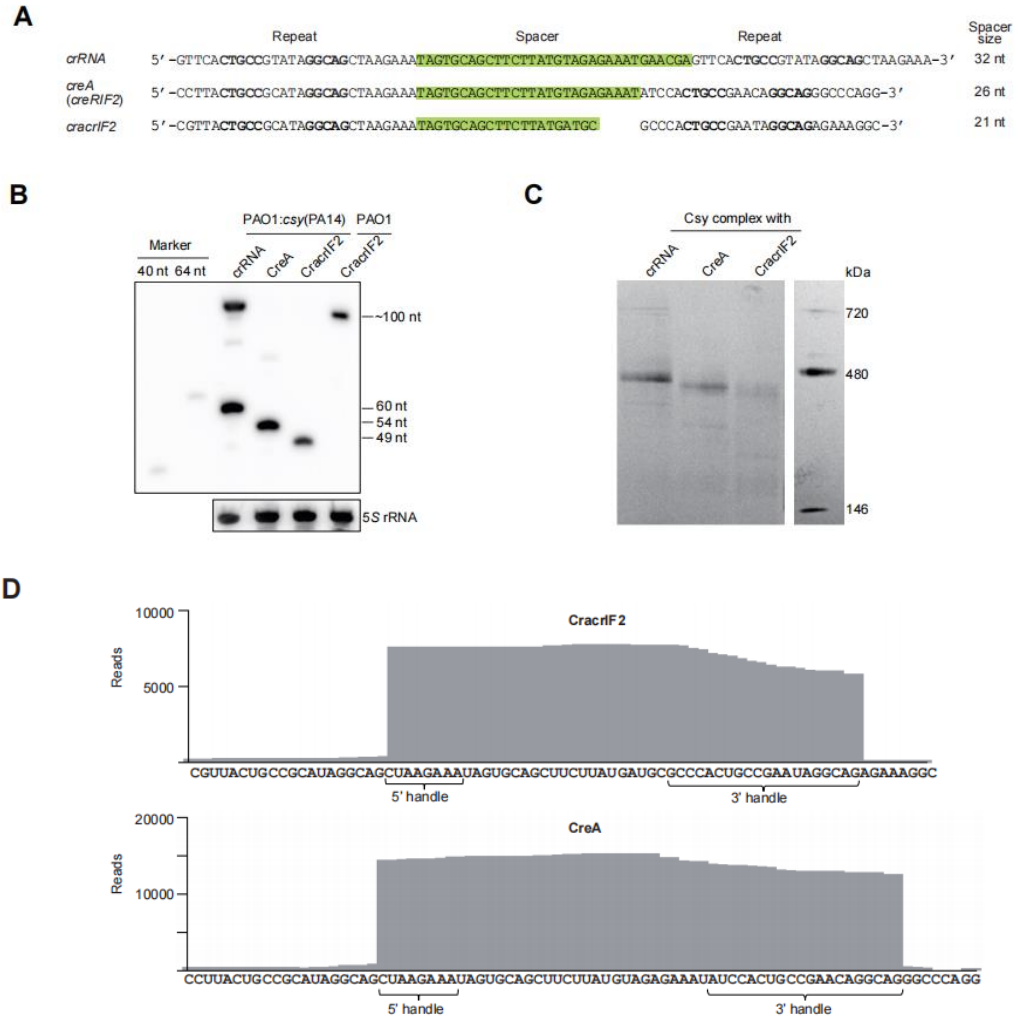

1189

1190

1191 **Fig. S5. Analysis of CracrIF2, CreA (CreRIF2), and a cognate crRNA, as well as the**
1192 **Csy complexes bound to different guide RNAs.**
1193 **(A)** Illustration of the sequence differences between *creA*, *cracrIF2*, and a synthetic mini-
1194 CRISPR encoding a cognate crRNA. The spacer region of crRNA was designed by
1195 appending five extra nucleotides (not complementary to the shared target site) to that of
1196 *creRIF2*, resulting a typical spacer size of 32 nt. (**B**) Northern blotting analysis of mature
1197 CreA, CracrIF2, and the cognate crRNA, demonstrating different sizes. These RNA
1198 molecules were expressed in PAO1 cells expressing the Csy proteins of PA14, and the total
1199 RNA samples were subjected to the blotting assay. As a control, PAO14 cells without Csy
1200 proteins producing the precursor RNAs of CracrIF2 were also included. 5*S* rRNA served
1201 as the internal control. Biotin-labeled single-stranded oligos (40 nt or 64 nt) served as
1202 markers. (**C**) Native PAGE analysis of the Csy complexes bound to CracrIF2, CreA, or the
1203 cognate crRNA. The Csy proteins and guide RNAs were co-expressed in *E. coli* BL21(DE3)
1204 and subsequently co-purified for analysis. (**D**) The 5' and 3' termini of CracrIF2 and CreA

1205 RNAs determined by small RNA sequencing.
1206

Fig. S6.

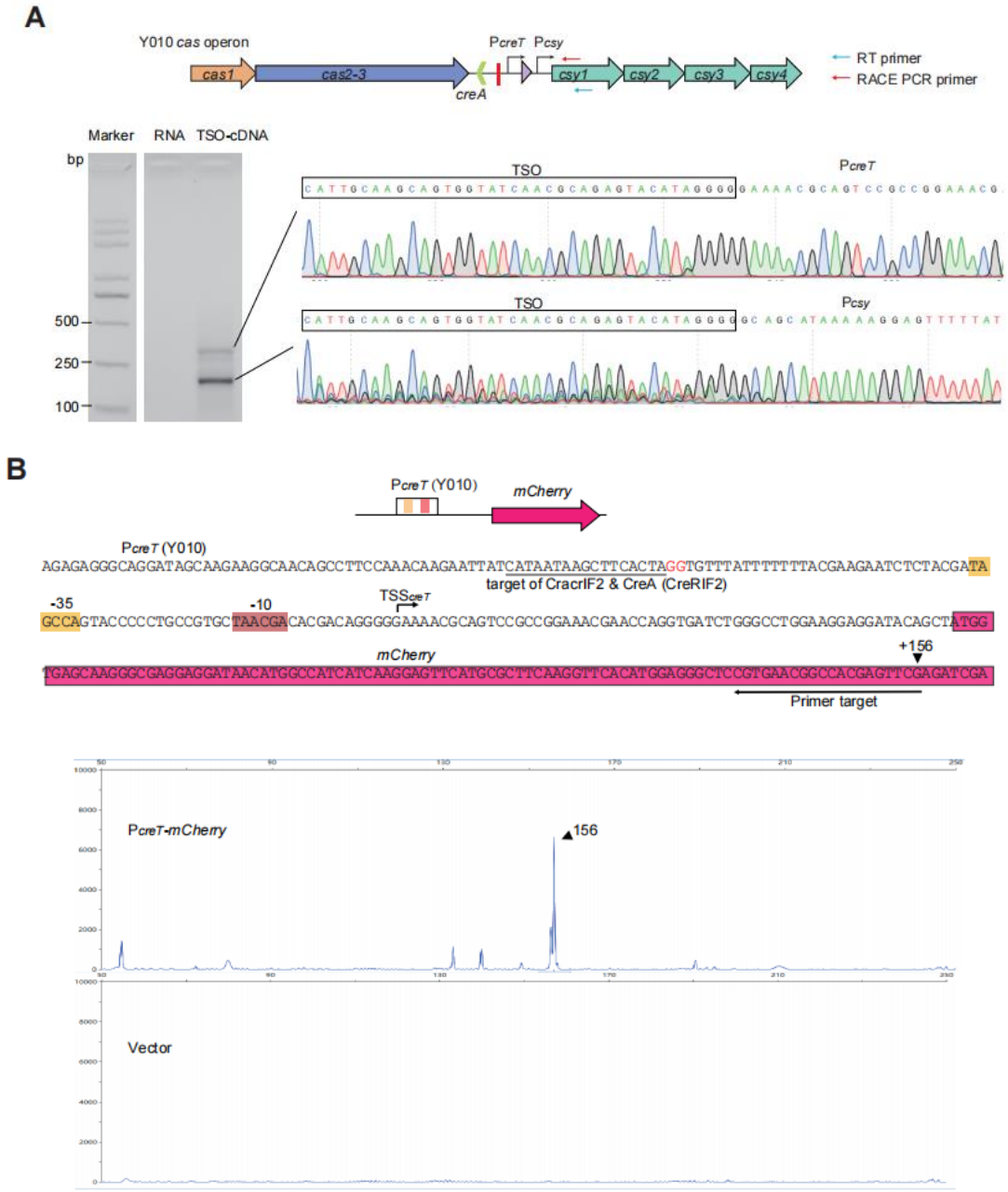

Fig. S6. Characterization of the *csy* promoter (P_{csy}) and *creT* promoter (P_{creT}) of NY010.

(**A**) Two transcription start sites of *csy* transcripts were determined by 5' RACE. cDNA was generated by reverse transcription (using RT primer), and subsequently used as the template for PCR reactions with a forward primer against the template switching oligo (TSO) and a reverse primer against *csy1* sequence (RACE PCR primer). DNase-treated RNA samples were used as the negative control. **(B)** Primer extension assay to confirm the

1218 TSS of Y010 P_{creT}. The P_{creT} DNA was first linked to an *mCherry* gene and then introduced
1219 into *P. aeruginosa* PAO1 cells, of which total RNA was extracted for primer extension. The
1220 primer was designed against the *mCherry* RNA transcript and 5'-labeled by FAM (see the
1221 Methods part). The cDNA products of primer extension assay were then subjected to
1222 fragment size analysis. PAO1 cells containing an empty vector served as a negative control.
1223 Promoter elements -10 and -35 are indicated. The target sequence of CracrIF2 or CreA
1224 RNAs are underlined, with the complementary nucleotides of PAM shown in red.
1225

Fig. S7.

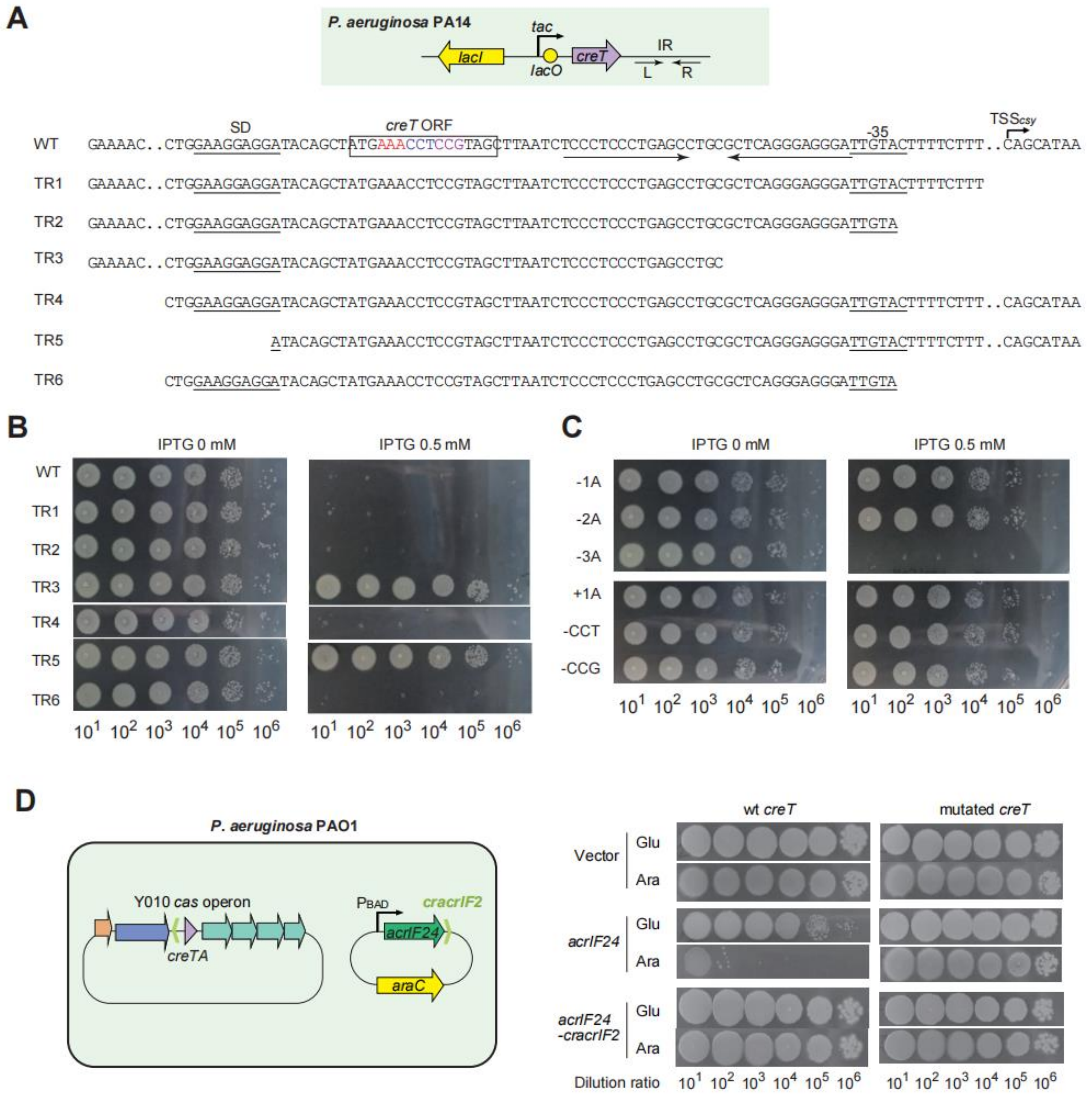

Fig. S7. Characterization of the CreT RNA toxin.

(**A**) Illustration showing the differently truncated DNA sequences (TR1-TR6) used to determine the minimal requirement to produce the toxicity of CreT. The critical elements, including a Shine-Dalgarno (SD) sequence, a mini-ORF, and a pair of inverted repeats (IR, labeled with two convergent arrows), are indicated along the wild-type (WT) sequence. The downstream -35 promoter element and TSS of *csy* genes are also denoted. The red nucleotides (AAA) were subjected to frameshift mutation analyses (panel **C**). The two proline codons (CCT and CCG) are highlighted in blue and purple, respectively. (**B**) Growth of PA14 cells expressing differently truncated *creT* genes. (**C**) Growth of PA14 cells when the mini-ORF of *creT* was differently mutated. The one (-1A), two (-2A), or all (-3A) the three nucleotides of the AAA codon (highlighted in red in panel **A**) were deleted for frameshift analysis. Addition of an extra adenine was also performed (+1A). The two

1241 proline codons were individually deleted in the -CCT and -CCG mutants. (**D**)Schematic
1242 representation (left) and results (right) of the assay to evaluate the ability of CracrIF2 RNAs
1243 to alleviate the CreTA cytoxicity that is triggered by AcrIF24 expression. AcrIF24 was
1244 individually expressed or co-transcribed with CracrIF2 under the control of the arabinose-
1245 inducible BAD promoter (P_{BAD}), with glucose used to suppress any basal activity of P_{BAD}.
1246 In the mutated *creT* control, the two critical proline codons were removed.
1247
1248

1249 **Fig. S8.**

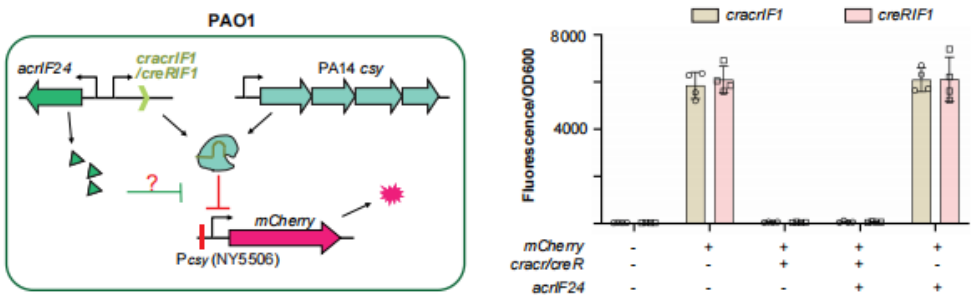

1250

1251 **Fig. S8. Both CrcrIF1 and CreRIF1 are resistant to AcrIF24.**
1252 Fluorescence intensity of PAO1 cells containing a plasmid expressing mCherry under the
1253 control of the Y5506 *csy* promoter (targeted by its corresponding CreRIF1 and the viral
1254 CracrIF1), a second plasmid expressing PA14 Csy proteins, and a third plasmid expressing
1255 CracrIF1 or CreRIF1 with or without the co-expression of AcrIF24.
1256
1257
1258

1259 **Fig. S9.**

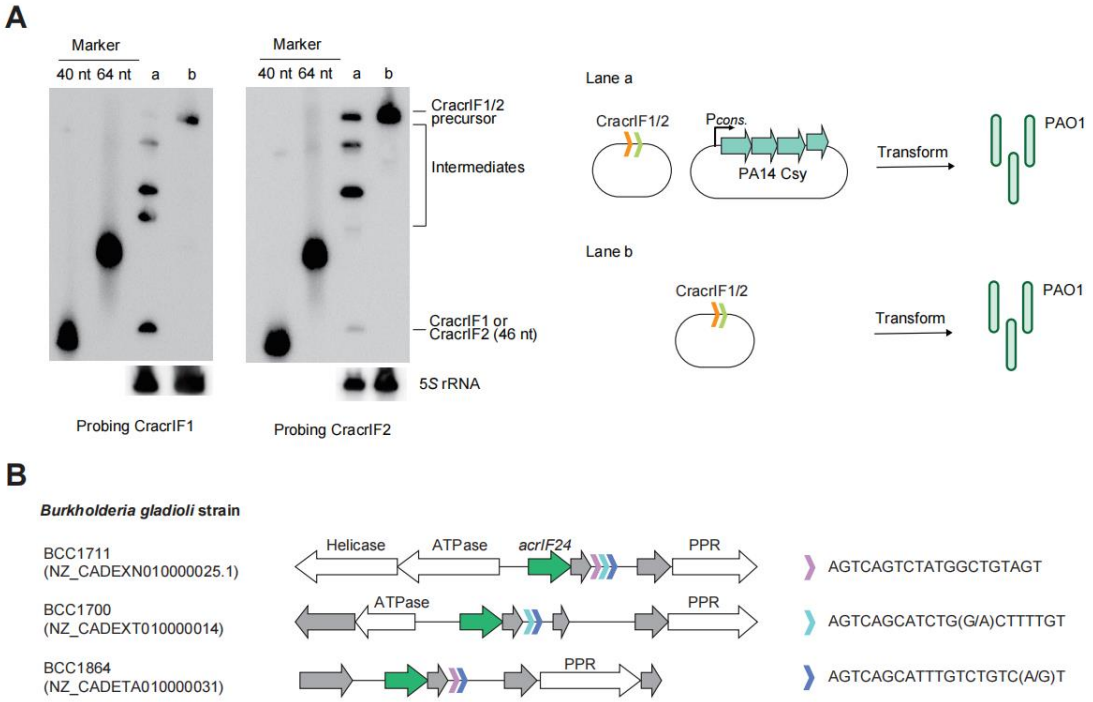

1260

1261 **Fig. S9. Cracr RNAs production from the *cracrIF1/2* array and other type I-F Cracr**
1262 **arrays from *Burkholderia gladioli* genomes.**
1263 (**A**) Northern blotting analysis of the CracrIF1 and CracrIF2 RNAs produced from their
1264 Cracr array. Experimental design is shown on the right. 5*S* rRNA served as the internal
1265 control. Biotin-labeled single-stranded oligos (40 nt or 64 nt) served as markers. (**B**) Three
1266 Cracr arrays carried by *B. gladioli* prophages. The nucleotide sequence of each ΨS is given
1267 on the right.
1268
1269

Fig. S10.

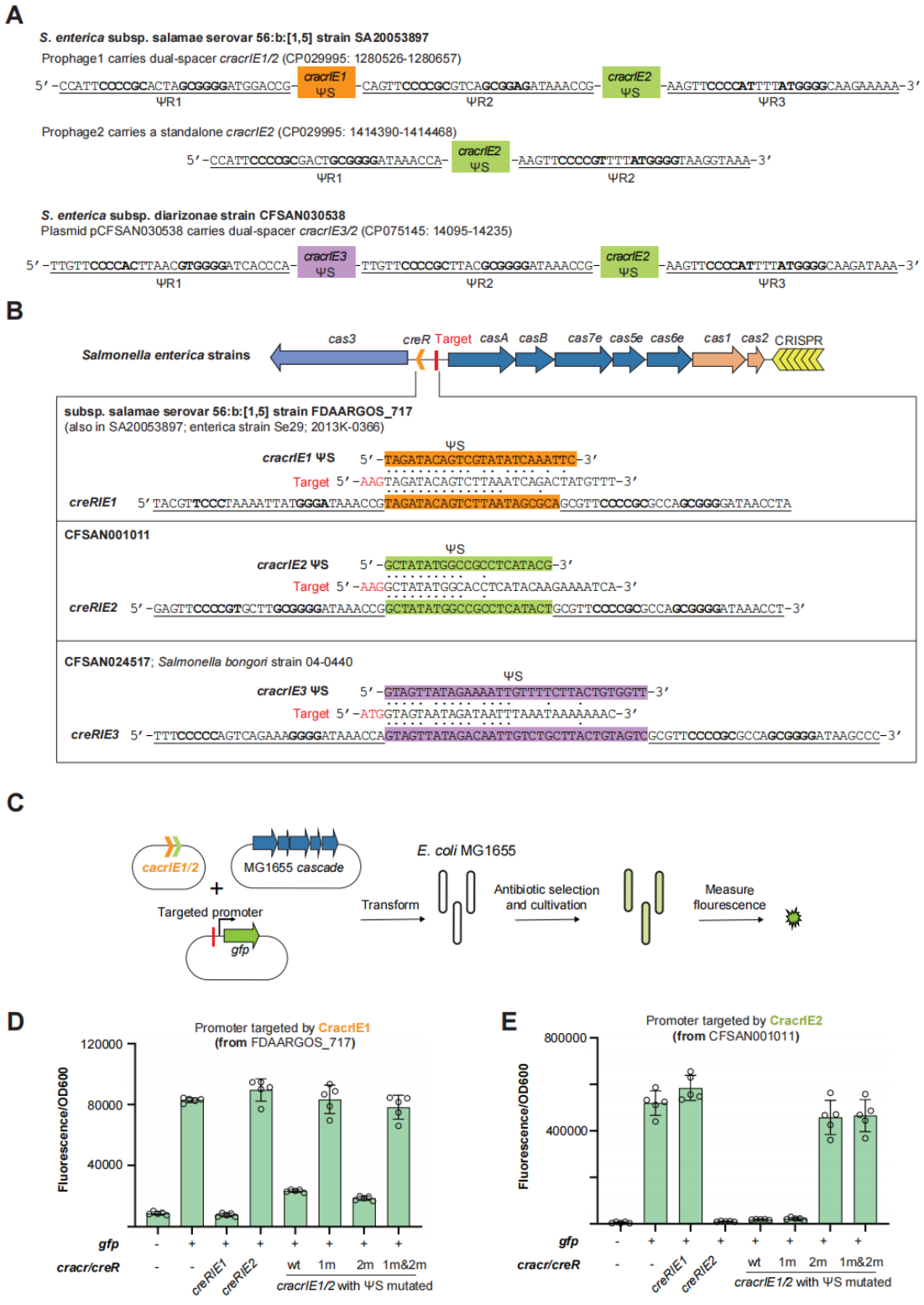

Fig. S10. Type I-E Cracr RNAs encoded by *Salmonella* MGEs and their regulatory activities.

1275 (**A**) Three related *cracr* genes or arrays carried by a prophage and a plasmid from
1276 *Salmonella*. The palindromic nucleotides within each ΨR sequence are shown in bold. **(B)**
1277 CRISPR-Cas systems that are potentially targeted by CracrIE1, CracrIE2, or CracrIE3. The
1278 PAM nucleotides are shown in red. Dots indicate identical nucleotides. (**C**) Illustration
1279 showing the experimental design to measure the inhibitory effect of the *cracrIE1/2* array
1280 on putative target promoters. (**D**) and (**E**) Green fluorescence intensity from *E. coli* cells
1281 with a *gfp* gene under the control of a putative promoter sequence that is targeted by
1282 CracrIE1 (D) or CracrIE2 (E). The first (1m) and second (2m) ΨS sequences of *cracrIE1/2*
1283 were individually mutated or simultaneously mutated (1m&2m). wt, wild-type. Error bars,
1284 mean±s.d. (n=5).
1285